POLITECNICO DI TORINO
Repository ISTITUZIONALE

Investigating strangeness enhancement with multiplicity in pp collisions using angular correlations

Original
Investigating strangeness enhancement with multiplicity in pp collisions using angular correlations / Null, N., Acharya, S., Adamová, D., Agarwal, A., Aglieri Rinella, G., Aglietta, L., Agnello, M., Agrawal, N., Ahammed, Z., Ahmad, S., Ahn, S.U., Ahuja, I., Akindinov, A., Akishina, V., Al-Turany, M., Aleksandrov, D., Alessandro, B., Alfanda, H.M., Alfaro Molina, R., Ali, B., et al.. - In: JOURNAL OF HIGH ENERGY PHYSICS. - ISSN 1029-8479. - STAMPA. - 2024:9(2024). [10.1007/jhep09(2024)204]

Availability:
This version is available at: 11583/3000892 since: 2025-06-14T08:12:35Z

Publisher:
Springer

Published
DOI:10.1007/jhep09(2024)204

Terms of use:

This article is made available under terms and conditions as specified in the corresponding bibliographic description in the repository

Publisher copyright

(Article begins on next page)

25 November 2026

Published for SISSA by Springer

Received: *June 15, 2024*
Accepted: *September 9, 2024*
Published: *September 27, 2024*

Investigating strangeness enhancement with multiplicity in pp collisions using angular correlations



The ALICE collaboration

E-mail: alice-publications@cern.ch

Abstract: A study of strange hadron production associated with hard scattering processes and with the underlying event is conducted to investigate the origin of the enhanced production of strange hadrons in small collision systems characterised by large charged-particle multiplicities. For this purpose, the production of the single-strange meson K^0_S and the double-strange baryon $\Xi^\pm$ is measured, in each event, in the azimuthal direction of the highest-p_T particle ("trigger" particle), related to hard scattering processes, and in the direction transverse to it in azimuth, associated with the underlying event, in pp collisions at $\sqrt{s} = 5.02\,\mathrm{TeV}$ and $\sqrt{s} = 13\,\mathrm{TeV}$ using the ALICE detector at the LHC. The per-trigger yields of K^0_S and $\Xi^\pm$ are dominated by the transverse-to-leading production (i.e., in the direction transverse to the trigger particle), whose contribution relative to the toward-leading production is observed to increase with the event charged-particle multiplicity. The transverse-to-leading and the toward-leading $\Xi^\pm/\mathrm{K}^0_\mathrm{S}$ yield ratios increase with the multiplicity of charged particles, suggesting that strangeness enhancement with multiplicity is associated with both hard scattering processes and the underlying event. The relative production of $\Xi^\pm$ with respect to K^0_S is higher in transverse-to-leading processes over the whole multiplicity interval covered by the measurement. The K^0_S and $\Xi^\pm$ per-trigger yields and yield ratios are compared with predictions of three different phenomenological models, namely Pythia8.2 with the Monash tune, Pythia8.2 with ropes and EPOS LHC. The comparison shows that none of them can quantitatively describe either the transverse-to-leading or the toward-leading yields of K^0_S and $\Xi^\pm$.

Keywords: Hadron-Hadron Scattering, Particle and Resonance Production, Particle Correlations and Fluctuations

ArXiv ePrint: 2405.14511

Open Access, Copyright CERN,
for the benefit of the ALICE Collaboration.
Article funded by SCOAP^3.

https://doi.org/10.1007/JHEP09(2024)204

JHEP09(2024)204

Contents

1 Introduction 1

2 Experimental setup and data selection 2

3 Analysis details 4
- 3.1 Trigger particle identification 4
- 3.2 Identification of K^0_S and $\Xi^{\pm}$ 5
- 3.3 The angular correlation function 6
- 3.4 Evaluation of the p_T spectra and integrated yields 9
- 3.5 Systematic uncertainties 11

4 Results 14

5 Summary and outlook 23

The ALICE collaboration 29

1 Introduction

The enhancement of strange hadron production in heavy-ion collisions with respect to minimum bias pp collisions was one of the first predicted signatures of quark-gluon plasma (QGP) formation [1–3]. This strangeness enhancement was first observed at the SPS [4–9] and was later measured in Au–Au collisions at RHIC [10] and in Pb–Pb collisions at the LHC [11]. The ALICE Collaboration further studied the production of strange hadrons in smaller collision systems, such as p–Pb [12–14] and pp collisions [15–21]. The results show that the ratios of (multi-)strange to non-strange hadron yields increase with the multiplicity of charged particles produced in the collision, reaching in high-multiplicity pp collisions values compatible with those measured in peripheral Pb–Pb collisions [22].

The smooth evolution of the ratios with multiplicity across different collision systems implies a common particle production mechanism in the different systems. This is also supported by other observables, such as "ridge"-like structures in the two-particle angular correlations at large pseudorapidity difference [23, 24] and non-vanishing anisotropic flow coefficients [25–27], which suggest the presence of collective effects in small collision systems [16]. These observations challenge the current understanding of hadronic collisions, as different particle production mechanisms are expected to be involved in the different collision systems [1].

Several theoretical approaches have attempted to describe the strange hadron production in hadronic collisions. A qualitative description of the experimental results has been achieved with different event generators, such as Pythia8 with colour ropes [28], HERWIG [29, 30] and EPOS LHC [31], which combine perturbative Quantum Chromodynamics (pQCD) calculations with phenomenological models for the description of hard and soft processes, respectively. A qualitative description of strange hadron production is also provided by

JHEP09(2024)204

the statistical hadronisation model, according to which the relative abundances of strange hadrons with respect to lighter flavours are diminished in small systems by a canonical suppression of the strangeness quantum numbers [32–35]. However, none of these theoretical approaches provides a consistent quantitative description of the multiplicity dependence of the hadron-to-pion ratios [15, 22, 36], indicating that the microscopic origin of strangeness enhancement with multiplicity in small collision systems remains an open issue.

One way to investigate this phenomenon consists in studying the strange hadron production associated with hard scattering processes and with the underlying event. Hard scattering processes are associated with high-energy parton shower (jet) hadronisation, whereas the underlying event consists of all the processes different from the hardest partonic interaction. The ALICE Collaboration has recently studied the p_{T} spectra of different (multi-)strange hadrons in jets and in the underlying event in minimum bias pp collisions at $\sqrt{s} = 7\,\mathrm{TeV}$ and $\sqrt{s} = 13\,\mathrm{TeV}$ and in p–Pb at $\sqrt{s_{\mathrm{NN}}} = 5.02\,\mathrm{TeV}$ [37, 38], using the anti-k_{T} algorithm [39, 40] for jet reconstruction. The results indicate that jet fragmentation alone is not sufficient to describe strange particle production in hadronic collisions at LHC energies and suggest that the baryon-over-meson yield ratios increase with multiplicity at intermediate p_{T} values [16] might be driven by particle production in the underlying event.

This paper presents a complementary measurement of strange hadron production associated with hard scattering processes and the underlying event as a function of the charged-particle multiplicity in pp collisions. The p_{T} spectra and the p_{T}-integrated yields of $\mathrm{K}^0_{\mathrm{S}}$ and $\Xi^{\pm}$ are measured at central rapidities in pp collisions at $\sqrt{s} = 5.02$ TeV and at $\sqrt{s} = 13$ TeV in the direction of the leading particle (trigger particle), which is considered to be a proxy for the jet axis, and in the direction transverse to the trigger particle, which is associated with the underlying event and might also receive a contribution from low-p_{T} jets (mini-jets). For this purpose, the angular correlations between trigger particles and $\mathrm{K}^0_{\mathrm{S}}$ ($\Xi^{\pm}$) are exploited. The single-strange meson $\mathrm{K}^0_{\mathrm{S}}$ and the double-strange baryon $\Xi^{\pm}$ are studied as they have a different strangeness content and therefore a different sensitivity to strangeness enhancement. In addition, these species receive a negligible feed-down from other particles, which simplifies the measurement of their yields. The $\mathrm{K}^0_{\mathrm{S}}$ and $\Xi^{\pm}$ per-trigger yields per unit $\Delta\eta\Delta\varphi$ are reported as a function of the charged-particle multiplicity and are compared with the predictions of three different phenomenological models, namely Pythia8.2 with the Monash 2013 tune [41], Pythia8.2 with ropes [28] and EPOS LHC [31].

The paper is organised as follows. Section 2 outlines the experimental setup and the data sample used for this measurement, section 3 presents the experimental details of the analysis along with the associated systematic uncertainties, and section 4 shows the per-trigger p_{T} spectra and p_{T}-integrated yields of $\mathrm{K}^0_{\mathrm{S}}$ and $\Xi^{\pm}$ as a function of the charged-particle multiplicity, together with their comparison with model predictions. Finally, the conclusions are drawn in section 5.

2 Experimental setup and data selection

The ALICE apparatus [42, 43] consists of central barrel detectors covering the pseudorapidity interval $|\eta| < 0.9$, a muon spectrometer covering $-4.0 < \eta < -2.5$, and a set of detectors at forward and backward rapidities used for triggering and event characterisation purposes.

JHEP09(2024)204

The central barrel detectors are positioned inside a solenoidal magnet providing a 0.5 T magnetic field along the beam axis and are used for primary vertex (PV) reconstruction, track reconstruction and charged-particle identification. The main detectors used for the analysis presented in this paper are the Inner Tracking System (ITS) [44], the Time Projection Chamber (TPC) [45], the Time Of Flight (TOF) detector [46], and the V0 detectors [47]. The ITS is the innermost detector of the ALICE experiment. The ITS used during the LHC Run 2 consisted of six cylindrical layers of silicon tracking detectors placed at a radial distance from the beam pipe between 3.9 and 43.0 cm. The two innermost layers of the ITS were equipped with Silicon Pixel Detectors (SPD), the two intermediate layers consisted of Silicon Drift Detectors (SDD), and the two outermost layers of Silicon Strip Detectors (SSD). The SPD was used to reconstruct the PV of the collision and the tracklets, short two-point track segments covering the pseudorapidity region $|\eta| < 1.2$. The other main functions of the ITS are the reconstruction of secondary vertices from weak decays and the tracking and identification of particles with momentum smaller than 200 MeV/c. The TPC is the main tracking detector of the central barrel. It is used for the identification of charged particles by measuring the specific ionisation energy loss dE/dx. The TPC has a cylindrical shape with an inner radius of 85 cm, an outer radius of 250 cm and an overall length along the beam direction of 5 m. It is filled with nearly 90 m^3 of gas mixture, consisting of Ar/CO_2 (88/12) in 2016 and 2018 and $Ne/CO_2/N_2$ (90/10/5) in 2017. It covers the pseudorapidity region of $|\eta| < 0.9$ for tracks with full radial length and provides full azimuthal acceptance. The TPC is radially segmented into "pad rows": tracks reconstructed with the TPC may consist of up to 159 points, each corresponding to one crossed pad row. The TOF detector is an array of multigap resistive plate chambers (MRPCs) covering the pseudorapidity range of $|\eta| \lesssim 0.9$ and providing full azimuthal acceptance. Its primary purpose is the identification of particles with intermediate momentum via the measurement of their time of flight. The V0 detector consists of two arrays of scintillation counters, V0A and V0C, placed at forward rapidity. The V0A is located at +3.3 m from the interaction point and covers the pseudorapidity range of $2.8 < \eta < 5.1$, whereas the V0C is placed on the opposite side at −0.9 m from the interaction point and covers the pseudorapidity range of $-3.7 < \eta < -1.7$. The V0 detector provides the minimum bias trigger in pp, p–Pb and Pb–Pb collisions. It is used to classify pp collisions in multiplicity percentile classes based on the total deposited charge (V0M amplitude).

The analysis presented in this paper was performed using pp collisions at $\sqrt{s} = 5.02$ TeV and $\sqrt{s} = 13$ TeV collected by the ALICE experiment during the LHC Run 2 data-taking campaign (2015–2018). Two samples of pp collisions at $\sqrt{s} = 13$ TeV were used: one collected with the minimum bias (MB) trigger, the other collected with the high multiplicity (HM) trigger. The MB trigger is provided by the combined signals in the V0A and V0C detectors. The HM trigger is activated online when the amplitude of the signal in the V0 detectors is above a predefined threshold and allows for the selection of events characterised by approximately 30 charged particles produced at midrapidity, i.e., four times more than those collected in minimum bias events (≈ 7). The sample of pp collisions at $\sqrt{s} = 5.02$ TeV was collected with the MB trigger, and consists of events characterised by approximately 6 charged particles produced at midrapidity.

To ensure uniform detector acceptance, the reconstructed PV position must lie within ±10 cm from the nominal interaction point in the beam direction. The contamination from in-

JHEP09(2024)204

bunch pileup events is removed by excluding events with multiple vertices reconstructed with the SPD. The background from beam-gas events is removed by using the timing information in the V0 detectors and the correlation between SPD tracklets and SPD clusters, as discussed in detail in ref. [43].

The MB events used for the trigger particle-K^0_S correlation analysis were collected in 2016 and 2017 and amount to about 1×10^9 good quality events. As $\Xi^\pm$ are approximately fifteen times less abundant than K^0_S, all MB events collected in 2016, 2017 and 2018 were used for the trigger particle-$\Xi^\pm$ correlation analysis, corresponding to 1.6×10^9 events after the quality selections. The sample of HM events at $\sqrt{s} = 13$ TeV consists of 4×10^8 selected events collected in 2016, 2017 and 2018. The sample of MB pp collisions at $\sqrt{s} = 5.02$ TeV consists of 9×10^8 good events recorded in 2017.

3 Analysis details

The selected events are divided into V0M multiplicity percentile classes defined starting from the distribution of the sum of the signal amplitudes measured with the two V0 detectors. Minimum bias events at $\sqrt{s} = 13$ TeV are divided into five multiplicity classes (0–5%, 5–10%, 10–30%, 30–50%, 50–100%): the 0–5% class, for example, contains the 5% of events with the highest V0M amplitude, while the 70–100% class contains the 30% of events with the smallest V0M amplitude. Once corrected for the V0M trigger efficiency, these ranges represent fractional intervals of the cross section of INEL > 0 events, defined as events having at least one charged particle produced in the pseudorapidity interval $|\eta| < 1$. The corrected intervals are respectively: 0–4.57%, 4.57–9.15%, 9.15–27.50%, 27.50–46.12%, 46.12–100%, respectively. The details about the correction procedure can be found in ref. [48]. High multiplicity events at $\sqrt{s} = 13$ TeV are selected in the multiplicity range 0–0.1%, which includes the 0.1% of the MB events characterised by the highest V0M amplitude. These events are further divided into three multiplicity classes: 0–0.01%, 0.01–0.05% and 0.05–0.1%, with the first one corresponding to 0–0.0091% of the INEL > 0 cross section, and the sum of the other two classes to 0.0091–0.0915%. The available number of MB events at $\sqrt{s} = 5.02$ TeV allows for the analysis to be performed only in two multiplicity classes (0–10%, 10–100%, corresponding to 0–9.15% and 9.15–100% of the INEL > 0 cross section, respectively), as at this energy the sample of MB events is smaller and the average strange hadron yields per event are smaller than those at $\sqrt{s} = 13$ TeV. For each V0M percentile class, the average multiplicity of charged particles produced at midrapidity in events containing a trigger particle, $\langle \mathrm{d}N_\mathrm{ch}/\mathrm{d}\eta \rangle_{|\eta|<0.5,\ p_\mathrm{T,trigg}>3\ \mathrm{GeV}/c}$, and its systematic uncertainties are computed using the technique described in ref. [48].

3.1 Trigger particle identification

In this analysis, a trigger particle is defined as the charged particle with the highest-p_T in a given event (leading particle), coming from the PV, produced in the pseudorapidity interval $|\eta| < 0.8$ and within the transverse momentum range $3 < p_\mathrm{T} < 15\,\mathrm{GeV}/c$. The minimum p_T threshold is applied to select particles originating from the hadronisation of hard scattering processes. An increase of the threshold value above $3\,\mathrm{GeV}/c$ would increase the contribution from particles originating from hard scattering processes. However, it would also decrease the

JHEP09(2024)204

number of events with a trigger particle, limiting the possibility of performing a multiplicity dependent measurement of the angular correlation between trigger particles and $\Xi^{\pm}$ baryons. The trigger particles are selected starting from the tracks reconstructed using the TPC and constrained to the PV. Only tracks in the $|\eta| < 0.8$ acceptance region, where full track reconstruction is provided, are accepted. Standard selections are applied: tracks are required to cross at least 80 out of 159 TPC pad rows and to be formed by more than 70 TPC clusters, where a cluster is the signal induced by the passage of the particle in a crossed pad row. In order not to have large gaps in the number of expected tracking points in the radial direction, the ratio of crossed pad rows N_{crossed} over findable clusters N_{findable} is required to be greater than 0.8. In order to reject the low-resolution tracks which pass through the edges of the TPC sectors, tracks with radial lengths smaller than 90 cm are discarded, and the ratio between the number of crossed pad rows and the radial track length is required to be greater than 0.8 cm^{-1}. In addition, a maximum p_{T} threshold of 15 GeV/c is applied to retain only tracks with p_{T} resolution better than 2%. This selection rejects less than 0.5% of tracks. Finally, the goodness-of-fit χ^2 per TPC cluster of the track fit in the TPC is required to be smaller than 4. To discard charged particles not originating from the PV, a selection on the distance of closest approach (DCA) of the track to the PV is applied both along the beam direction z (DCA_z) and in the perpendicular plane (DCA_{xy}):

$$|\text{DCA}_z| < 0.04 \text{ cm} \, , \, |\text{DCA}_{xy}| < \left(0.0105 + \frac{0.035}{[p_{\text{T}}/(\text{GeV}/c)]^{1.1}}\right) \text{ cm}.$$

The p_{T}-dependent selection on the DCA_{xy} allows for selecting tracks within 7σ from the interaction vertex in the transverse plane, where σ is the resolution with which the DCA_{xy} is measured.

The fraction of good-quality events containing a trigger particle increases with the event multiplicity, from approximately 2% in the 50–100% V0M class to 50% in the highest multiplicity class 0–0.01%, as it is more likely to find a high-p_{T} track in events characterised by a larger multiplicity of charged particles.

3.2 Identification of K^0_{S} and $\Xi^{\pm}$

The strange hadrons K^0_{S}, Ξ^- and Ξ^+ (in the following $\Xi^{\pm}$) are identified in the pseudorapidity range of $|\eta| < 0.8$ via invariant mass analysis techniques, exploiting the topology of their weak decays into charged hadrons [49]:

$\text{K}^0_{\text{S}} \to \pi^+\pi^-$	B.R. $= (69.20 \pm 0.05)\%$
$\Xi^- \to \Lambda\pi^- \to \text{p}\pi^-\pi^-(\Xi^+ \to \overline{\Lambda}\pi^+ \to \overline{\text{p}}\pi^+\pi^+)$	B.R.$(\Xi^- \to \Lambda\pi^-) = (99.887 \pm 0.035)\%$
	B.R.$(\Lambda \to \text{p}\pi^-) = (63.9 \pm 0.5)\%$.

The charged daughter tracks of K^0_{S} and $\Xi^{\pm}$ candidates are selected in the pseudorapidity range of $|\eta| < 0.8$, and are required to satisfy the same track quality criteria applied for the trigger particle selection. Daughter tracks in the whole p_{T} interval are identified by requiring the specific ionisation energy loss $\text{d}E/\text{d}x$ measured in the TPC to be compatible with the expected theoretical value within $\pm 3\sigma$, where σ is related to the resolution with which $\text{d}E/\text{d}x$ is measured. In addition, daughter tracks are required not to be associated with a "kink

JHEP09(2024)204

topology" [50], which is characteristic of the decay of charged kaons. The combinatorial background is suppressed by applying standard topological selections (see ref. [18]), listed in table 1. A selection on the proper lifetime τ of K^0_S and $\Xi^\pm$ candidates is also applied. The proper lifetime is calculated as $\tau = d \times m/|\vec{p}|$, where m is the nominal mass of the considered particle, $|\vec{p}|$ is the magnitude of the reconstructed momentum, and d is the distance of the reconstructed secondary decay vertex from the primary one. In order to identify $\Xi^\pm$, the invariant mass of the daughter (anti-)Λ is required to differ from the nominal mass value of the Λ by less than $6\,\mathrm{MeV}/c^2$, according to the (anti-)Λ invariant mass resolution. The background from (anti-)Λ in the K^0_S sample is suppressed by rejecting the K^0_S candidates whose invariant mass calculated under the pπ assumption for the daughter tracks lies within $\pm 5\,\mathrm{MeV}/c^2$ from the nominal Λ mass. Similarly, the background from $\Omega^\pm$ in the cascade sample is tackled by rejecting the cascade candidates whose invariant mass calculated under the ΛK assumption for the daughter particles lies within $\pm 5\,\mathrm{MeV}/c^2$ from the nominal Ω mass. The width of the rejected region is determined according to the invariant mass resolution σ of the competing candidate, and corresponds to approximately $\pm 3\sigma$. Finally, to reduce the out-of-bunch pileup background caused by tracks from other bunch crossings within the TPC integration time, at least one of the daughter tracks is required to have a hit in the TOF or the SPD.

The signal extraction is performed as a function of p_T. The invariant mass distributions of K^0_S and $\Xi^\pm$ candidates are fitted with the sum of two Gaussian functions, used to take into account the invariant mass resolution of the signal peak, and a first-degree polynomial, used to describe the background. A "peak" region is defined within $\pm 4\sigma$ from μ, where μ and σ are the average mean value and width of the two Gaussian functions, respectively. For each candidate, "sideband" regions are defined: the sidebands of the K^0_S ($\Xi^\pm$) invariant mass distributions are defined as the intervals $\mu - 10\sigma < m_{\pi^+\pi^-}(m_{\pi\Lambda}) < \mu - 4\sigma$ and $\mu + 4\sigma < m_{\pi^+\pi^-}(m_{\pi\Lambda}) < \mu + 10\sigma$. The purity of the K^0_S and $\Xi^\pm$ candidates samples, defined as the ratio between the signal and the total number of candidates in the invariant mass range within $\pm 4\sigma$ from μ, is larger than 0.95 and 0.89 for K^0_S and $\Xi^\pm$, respectively.

3.3 The angular correlation function

The angular correlation between trigger particles, denoted as "h", and associated particles, i.e. the K^0_S ($\Xi^\pm$) candidates with an invariant mass within 4σ from the average mean value μ of the Gaussian fit functions, is expressed as a function of the pseudorapidity difference $\Delta\eta$ and the azimuthal angle difference $\Delta\varphi$ between the trigger and associated particles. Examples of the angular correlation distribution $\mathrm{d}^2N_\mathrm{assoc}(\Delta\eta, \Delta\varphi)/\mathrm{d}\Delta\eta\mathrm{d}\Delta\varphi$ of h-K^0_S and h-$\Xi^\pm$pairs produced in pp collisions at $\sqrt{s} = 13$ TeV are shown in the left panel of figures 1 and 2, respectively. The distributions show a near-side peak centred at $(\Delta\eta, \Delta\varphi) = (0, 0)$ which is associated with h-K^0_S and h-$\Xi^\pm$ pairs fragmented within the same jet. The distributions are corrected by the efficiency×acceptance×B.R. of associated particles ϵ_assoc computed using a Monte Carlo simulation based on Pythia8.2 with the Monash 2013 tune [41] for the generation of events and on Geant 4 [51] for the description of the propagation of particles through the material of the detector. The term ϵ_assoc is calculated in events with a trigger particle identified by applying the selections described in section 3.1. It increases with p_T, reaching a saturation value of about 35% and 25% at $p_\mathrm{T} = 3$ and $4\,\mathrm{GeV}/c$ for K^0_S and $\Xi^\pm$,

JHEP09(2024)204

Daughter-track selections	
Number of TPC clusters	> 70
χ^2/ndf	< 4
Number of TPC crossed pad rows $N_{\rm crossed}$	> 80
$N_{\rm crossed}/N_{\rm findable}$	> 0.8
Track length $l_{\rm TPC}$ in the TPC	> 90 cm
$N_{\rm crossed}/l_{\rm TPC}$	> 0.8 cm^{-1}
Rejection of kink topology	Yes
$\lvert\eta\rvert$	< 0.8
$\mathrm{d}E/\mathrm{d}x$ measured in the TPC	$< 3\sigma$
At least one daughter track has a hit in the SPD or in the TOF	Yes
K^0_S-topological-variable selections	
DCA daughter tracks to PV	> 0.06 cm
DCA between daughter tracks	$< 1\sigma$
$\cos(\theta_\mathrm{P})$	> 0.995
DCA K^0_S to PV	< 0.5 cm
K^0_S decay radius	> 0.5 cm
$\Xi^\pm$-topological-variable selections	
DCA meson daughter to PV	> 0.04 cm
DCA baryon daughter to PV	> 0.03 cm
DCA bachelor to PV	> 0.04 cm
DCA between daughter tracks of the Λ	$< 1.5\sigma$
$\cos(\theta_\mathrm{P})$ (of $\Xi^\pm$ to PV)	> 0.995
$\cos(\theta_\mathrm{P})$ (of (anti-)Λ to $\Xi^\pm$ decay vertex)	> 0.97
DCA between bachelor and (anti-)Λ	< 0.8 cm
DCA Λ to PV	> 0.06 cm
(anti-)Λ decay radius	> 1.1 cm
$\Xi^\pm$ decay radius	> 0.5 cm
K^0_S-candidate selections	
$\lvert\eta_{\mathrm{K}^0_\mathrm{S}}\rvert$	< 0.8
$\lvert\mathrm{m}_{\pi\mathrm{p}} - \mathrm{m}_\Lambda\rvert$	$> 5\,\mathrm{MeV}/c^2$
Proper lifetime τ	< 20 cm$/c$ ($\simeq 7.5\langle\tau_{\mathrm{K}^0_\mathrm{S}}\rangle$)
$\Xi^\pm$-candidate selections	
$\lvert\eta_{\Xi^\pm}\rvert$	< 0.8
$\lvert\mathrm{m}_{\pi\mathrm{p}} - \mathrm{m}_\Lambda\rvert$	$< 6\,\mathrm{MeV}/c^2$
$\lvert\mathrm{m}_{\mathrm{K}\Lambda} - \mathrm{m}_\Omega\rvert$	$> 5\,\mathrm{MeV}/c^2$
Proper lifetime τ	< 14.73 cm$/c$ ($= 3\langle\tau_{\Xi^\pm}\rangle$)

Table 1. Daughter-track quality selections, topological and kinematic selections applied to K^0_S and $\Xi^\pm$ candidates. The symbol θ_P stands for the pointing angle, i.e. the angle between the reconstructed momentum vector of the K^0_S and $\Xi^\pm$ candidates and the line connecting the primary to the secondary vertex. All other symbols are explained in the text.

JHEP09(2024)204

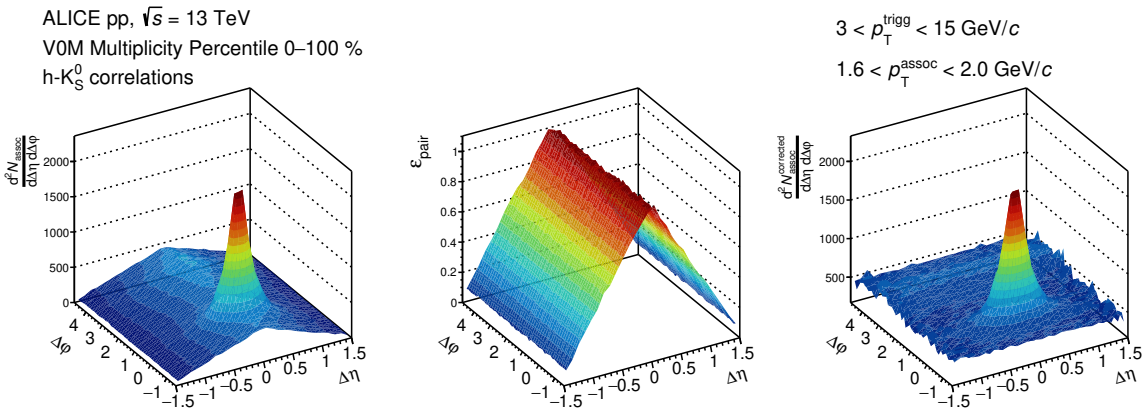

Figure 1. (left) Example of angular correlation distribution between trigger and K^0_S found in the same collision. (centre) Acceptance correction of trigger-K^0_S pairs. (right) Angular correlation distribution divided by the pair acceptance.

respectively. For K^0_S, ϵ_{assoc} increases with decreasing charged-particle multiplicity, varying by about 10% from the 0–5% to the 50–100% V0M multiplicity classes, whereas for $\Xi^{\pm}$, because of the different decay topology, it does not depend on multiplicity. For both particles, ϵ_{assoc} is computed in each multiplicity class and as a function of η and p_T, and is applied as a weight factor to each entry of the angular correlation distribution.

The angular correlation distributions (left panel of figures 1 and 2) exhibit a triangular shape in $\Delta\eta$, which is related to the geometrical acceptance of the trigger-associated particle pairs. It is corrected for by the pair acceptance ϵ_{pair}, calculated with the mixed-event method, which correlates the trigger particle found in one event with the associated particles produced in different events. These events are required to have similar characteristics, namely to lie in the same multiplicity class, to have the z-coordinate of the PV differing by less than 2 cm, and to contain a trigger particle. Each entry of the mixed-event angular correlation distribution is weighed with $1/\epsilon_{assoc}$, to take into account the η dependence of the associated particle efficiency. As shown in the central plot of figures 1 and 2, the mixed-event angular correlation distribution has a triangular shape in $\Delta\eta$, determined by the η acceptance. In contrast, it shows no dependence on $\Delta\varphi$, as a consequence of the cylindrical symmetry of the detector. To obtain the pair acceptance, the mixed-event distribution is normalised to unity at $\Delta\eta \simeq 0$, where all particle pairs are assumed to be accepted. The raw angular correlation distributions are divided by the pair acceptance to retain the genuine physical correlations in such pair-acceptance window $d^2N^{corrected}_{assoc}(\Delta\eta, \Delta\varphi)/d\Delta\eta d\Delta\varphi$, shown in the right panel of figures 1 and 2. The pair acceptance is computed in each multiplicity class. Since the h-$\Xi^{\pm}$acceptance does not show any multiplicity dependence within the statistical uncertainty, the correction is performed using the pair acceptance computed in the 0-100% multiplicity class, in order to reduce statistical fluctuations.

JHEP09(2024)204

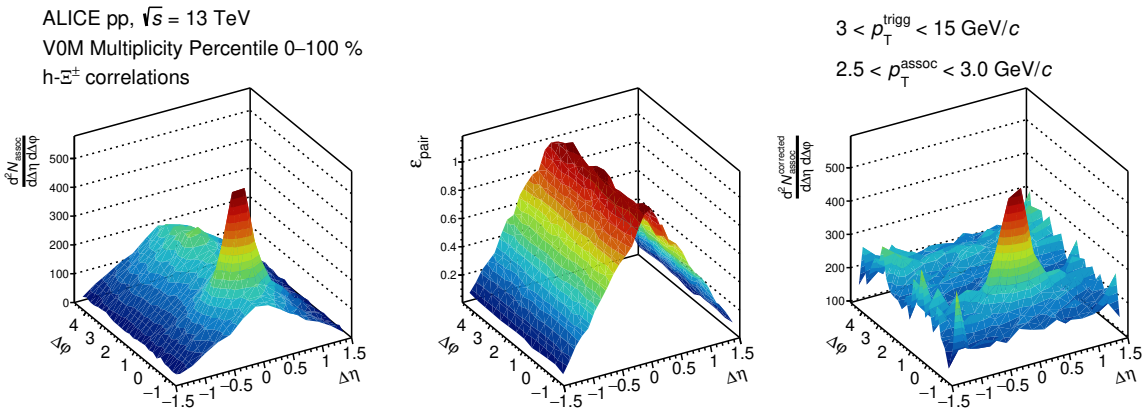

Figure 2. (left) Example of angular correlation distribution between trigger and $\Xi^{\pm}$ found in the same collision. (centre) Acceptance correction of trigger-$\Xi^{\pm}$ pairs. (right) Angular correlation distribution divided by the pair acceptance.

3.4 Evaluation of the p_{T} spectra and integrated yields

The corrected angular correlation distributions $\mathrm{d}^2N_{\mathrm{assoc}}^{\mathrm{corrected}}(\Delta\eta, \Delta\varphi)/\mathrm{d}\Delta\eta\mathrm{d}\Delta\varphi$ (right panel of figures 1 and 2) are projected onto the $\Delta\varphi$ axis. The $\Delta\varphi$ projections are corrected for the contribution of the combinatorial background due to candidates which are not $\mathrm{K}^0_{\mathrm{S}}$ ($\Xi^{\pm}$). The standard procedure, which is applied to $\mathrm{K}^0_{\mathrm{S}}$ in all samples and to $\Xi^{\pm}$ in the HM sample, consists of subtracting the angular correlations obtained using $\mathrm{K}^0_{\mathrm{S}}$ ($\Xi^{\pm}$) candidates in the "sidebands" of the invariant mass distributions from those obtained from the peak region. Before subtraction, the angular correlation obtained from the sidebands is divided by the integral of the invariant mass distribution in the sidebands regions and multiplied by the integral of the background fit function in the signal region in order to take into account the purity of the $\mathrm{K}^0_{\mathrm{S}}$ and $\Xi^{\pm}$ samples. A different procedure is applied to take into account the contribution of misidentified $\Xi^{\pm}$ in minimum bias pp collisions at $\sqrt{s} = 13$ TeV and at $\sqrt{s} = 5.02$ TeV, since these samples do not contain enough events to compute the h-$\Xi^{\pm}$angular correlation distributions from the sidebands regions. In this case, the $\Delta\varphi$ projections are multiplied by the purity of the sample of $\Xi^{\pm}$ candidates. This procedure assumes that the angular correlation distributions for background candidates have the same shape as for signal candidates. A systematic uncertainty is applied to take into account any difference with respect to the standard procedure, as described in section 3.5.

In addition, the $\Delta\varphi$ projections are corrected for the fraction of feed-down $\mathrm{K}^0_{\mathrm{S}}$ ($\Xi^{\pm}$). For this purpose, the distributions are multiplied by $(1 - F_{\mathrm{NP}})$, where F_{NP} is the fraction of non-primary $\mathrm{K}^0_{\mathrm{S}}$ ($\Xi^{\pm}$) calculated using Monte Carlo simulations. This procedure is based on the assumption that the angular correlation for feed-down particles has the same shape as the angular correlation for primary strange hadrons. This correction has a negligible impact since in the p_{T} ranges considered in this analysis $F_{\mathrm{NP}} \sim 0.5\%$ for $\Xi^{\pm}$ and $F_{\mathrm{NP}} < 0.05\%$ for $\mathrm{K}^0_{\mathrm{S}}$.

The associated particle yields are computed by integrating the $\Delta\varphi$ projections and are divided by the width of the $\Delta\eta\Delta\varphi$ region from which they are extracted. The toward-leading production is extracted from the region ($|\Delta\eta| < 0.86$, $|\Delta\varphi| < 1.1$), chosen to

JHEP09(2024)204

include the whole near-side peak. The transverse-to-leading production is extracted from ($0.86 < |\Delta\eta| < 1.2$, $0.96 < \Delta\varphi < 1.8$): this region is chosen to exclude the away-side peak associated with the recoil jet, whose contribution is situated around $\Delta\varphi \sim \pi$ and is elongated over the whole $\Delta\eta$ interval, and to exclude any possible residual near-side peak contribution in the region around $\Delta\varphi \sim 0$. Finally, the full yield is obtained from the whole $\Delta\eta\Delta\varphi$ region ($|\Delta\eta| < 1.2$, $-\pi/2 < \Delta\varphi < 3/2\pi$).

To obtain the toward-leading yield, the contribution of the underlying event is subtracted from the toward-leading $\Delta\varphi$ projections. An estimate of the underlying event contribution is provided by the long-range $\Delta\varphi$ projections obtained from the $0.86 < |\Delta\eta| < 1.2$ region and scaled to take into account the different $\Delta\eta$ widths of the two regions. This procedure cannot be applied to extract the toward-leading yield of $\Xi^{\pm}$ with $p_{\mathrm{T}} \lesssim 2\,\mathrm{GeV}/c$ in the minimum bias samples because of the large statistical uncertainties affecting the long-range $\Delta\varphi$ projections. To overcome this issue, the angular correlation between charged particles with $0.15 < p_{\mathrm{T}} < 2.5\,\mathrm{GeV}/c$ and $\Xi^{\pm}$ candidates is computed, and the $\Delta\varphi$ projections obtained from the $0.86 < |\Delta\eta| < 1.2$ region are used as estimates of the underlying event, after being scaled in order to match the $|\Delta\eta| < 0.86$ projections in the interval $1 \lesssim \Delta\varphi \lesssim 2$. These projections do not suffer from large statistical uncertainties. They are observed to be compatible within uncertainties with the default distributions in the $-\pi/2 < \Delta\varphi < \pi/2$ interval, where the near-side peak lies. A systematic uncertainty related to this procedure is evaluated as described in section 3.5.

The per-trigger yields per unit $\Delta\eta\Delta\varphi$, from now on referred to as "yields", are corrected by an additional normalisation factor C_{norm} in order to obtain the fully corrected p_{T} spectra $\left(\frac{1}{N_{\mathrm{trigg}}}\frac{1}{\Delta\eta\Delta\varphi}\frac{\mathrm{d}N}{\mathrm{d}p_{\mathrm{T}}}\right)$ in the three different regions:

$$\frac{1}{N_{\mathrm{trigg}}}\frac{1}{\Delta\eta\Delta\varphi}\frac{\mathrm{d}N}{\mathrm{d}p_{\mathrm{T}}} = \frac{1}{N_{\mathrm{trigg}}}\frac{1}{\Delta\eta\Delta\varphi}\frac{1}{\Delta p_{\mathrm{T}}}C_{\mathrm{norm}}\int_{\Delta\varphi}\frac{\mathrm{d}N_{\mathrm{assoc}}^{\mathrm{corrected}}}{\mathrm{d}\Delta\varphi}\mathrm{d}\Delta\varphi, \tag{3.1}$$

where N_{trigg} is the number of trigger particles in a given V0M multiplicity class and C_{norm} considers the efficiency with which events with a trigger particle are selected. The normalisation factor C_{norm} is computed using a Monte Carlo simulation and depends on the efficiency of trigger particle reconstruction and the difference between the $\mathrm{K}^0_{\mathrm{S}}$ ($\Xi^{\pm}$) spectra measured in events with a reconstructed trigger particle and events with a generated trigger particle. This correction factor is compatible with one for the toward-leading spectra, whereas it decreases with p_{T} for full and transverse-to-leading spectra, reaching a saturation value of about 0.98 at $p_{\mathrm{T}} > 3\,\mathrm{GeV}/c$ for both $\mathrm{K}^0_{\mathrm{S}}$ and $\Xi^{\pm}$.

To compute the p_{T}-integrated yields, the spectra are fitted with four different functions used to extrapolate the yield in the unmeasured p_{T} interval. The extrapolated yield is the average obtained from the four different fit functions: the Lévi-Tsallis [52], the Boltzmann, the Fermi-Dirac, and the m_{T}-exponential functions [18]. The extrapolated fraction of the $\mathrm{K}^0_{\mathrm{S}}$ yield amounts up to approximately 1% of the total yield for full and transverse-to-leading production and to approximately 8% for toward-leading production, because of the larger unmeasured p_{T} interval. The extrapolated fraction of the $\Xi^{\pm}$ yield varies between 10% and 40% for full and transverse-to-leading production and between 20% and 35% for toward-leading production, depending on the multiplicity class. It is worth mentioning that the extrapolated

JHEP09(2024)204

fraction for transverse-to-leading yields is larger than for toward-leading yields in the same unmeasured p_{T} interval, as transverse-to-leading spectra are softer.

3.5 Systematic uncertainties

Several systematic uncertainties affecting the measurement of the full, transverse-to-leading and toward-leading p_{T} spectra are investigated. All the considered sources of systematic uncertainties are reported in table 2 for $\mathrm{K}^0_{\mathrm{S}}$ (top) and $\Xi^{\pm}$ (bottom) p_{T} spectra, together with the relative uncertainty associated with each of the sources at three different p_{T} values in minimum bias pp collisions at $\sqrt{s} = 13$ TeV.

The topological selections are varied to take into account the differences between the distributions of the topological variables in the data and in the Monte Carlo simulation used to compute the $\mathrm{K}^0_{\mathrm{S}}$ and $\Xi^{\pm}$ acceptance×efficiencies. The systematic uncertainty is evaluated from the distribution of the fully corrected yields obtained by randomly changing the topological selections within ranges leading to a maximum variation of about ±2% in the raw signal yields when one single topological variable is varied. The relative systematic uncertainty depends on the multiplicity class. Overall, it is smaller than 2% (4%) for the transverse-to-leading and full p_{T} spectra of $\mathrm{K}^0_{\mathrm{S}}$ ($\Xi^{\pm}$). For the toward-leading spectra of $\mathrm{K}^0_{\mathrm{S}}$ ($\Xi^{\pm}$) it reaches values up to 8% at $p_{\mathrm{T}} < 1$ (2) GeV/c, decreasing with increasing p_{T}. This source of uncertainty represents the dominant one for the toward-leading spectra.

The effect of a different fraction of non-primary charged particles in the sample of trigger particles is evaluated by varying the selection applied to the DCA_z of the trigger particles. The systematic uncertainty is extracted from the distribution of the fully corrected yields obtained by randomly changing the DCA_z selection within the $(0, 2)$ cm range. The relative uncertainty associated with this source is smaller than 0.2% for full and transverse-to-leading production, and smaller than 0.5% for toward-leading production: it represents the smallest contribution to the total systematic uncertainty.

The systematic uncertainty associated with the choice of the $\Delta\eta$ region is assessed by changing the default boundaries of the $\Delta\eta$ regions by about +10%. The boundaries are not decreased below the default value, in order not to exclude any part of the near-side peak. The results are compared with those obtained with the default ranges. The variations are significant according to the Barlow criterion [53], with a 2σ threshold in at least four out of ten $\Delta\varphi$ intervals, indicating that the probability that they are due to statistical fluctuations is smaller than 0.1%. For both $\mathrm{K}^0_{\mathrm{S}}$ and $\Xi^{\pm}$, the relative systematic uncertainty of the transverse-to-leading spectra is smaller than 2%, whereas for the toward-leading spectra it decreases with p_{T} from at most 6% for $p_{\mathrm{T}} < 1(2)\,\mathrm{GeV}/c$ for $\mathrm{K}^0_{\mathrm{S}}$ ($\Xi^{\pm}$) to less than 2% for $p_{\mathrm{T}} > 3\,\mathrm{GeV}/c$. The full yield, which by definition is obtained from the region ($|\Delta\eta| < 1.2$, $-\pi/2 < \Delta\varphi < 3/2\pi$), is not affected by this source of systematic uncertainty.

Similarly, the systematic uncertainty related to the choice of the $\Delta\varphi$ interval is assessed by changing the default boundaries of the $\Delta\varphi$ regions by about ±10%. For both $\mathrm{K}^0_{\mathrm{S}}$ and $\Xi^{\pm}$, the variations of the transverse-to-leading $\Delta\varphi$ interval are significant according to the Barlow check with a 2σ threshold in at least three p_{T} intervals. The relative uncertainty, computed taking into account only the significant variations, increases with p_{T} up to 2% for both particles. The variations of the toward-leading yields are significant for $\mathrm{K}^0_{\mathrm{S}}$ in

JHEP09(2024)204

Hadron	K^0_S		
p_T (GeV/c)	≈0.6	≈1.8	≈3.5
Topological selections:*			
Full	0.3%	0.3%	0.3%
Transverse-to-leading	0.5%	0.5%	0.5%
Toward-leading	2%	2%	1%
Trigger particle DCA_z selection	0.1%	0.07%	0.05%
Choice of $\Delta\eta$ region*	0.3% (2%)	0.5% (1.2%)	0.7% (0.7%)
Choice of $\Delta\varphi$ region*	0.7% (2.5%)	0.7% (0.7%)	1.2% (0.2%)
Background fit function	0.1%	0.3%	0.5%
Choice of Monte Carlo	1%	1%	1%
Material budget	2%	0.2%	0.4%
Residual in-bunch pileup	2%	2%	2%
Out-of-bunch pileup track rejection	1.2%	1.2%	1.2%
Total	**3% (5%)**	**3% (3.5%)**	**2.5% (3%)**

Hadron	$\Xi^{\pm}$		
p_T (GeV/c)	≈0.6	≈1.8	≈3.5
Topological selections:*			
Full	1%	0.1%	0.2%
Transverse-to-leading	3.0%	0.6%	0.5%
Toward-leading	–	5%	3%
Trigger particle DCA_z selection	0.1%	0.07%	0.05%
Choice of $\Delta\eta$ region*	2%	1% (2%)	1% (1%)
Choice of $\Delta\varphi$ region*	0.9%	1% (–)	1.2% (–)
Background fit function	0.5%	0.5%	0.5%
Misidentified $\Xi^{\pm}$ subtraction	0.8%	0.4% (2.5%)	0.3% (1.2%)
Out-of-jet subtraction	–	5%	–
Material budget	2%	2%	2%
Residual in-bunch pileup	2%	2%	2%
Out-of-bunch pileup track rejection	2%	2%	2%
Total	**5%**	**3% (8%)**	**3% (4%)**

Table 2. Summary of the relative systematic uncertainties of the K^0_S (top) and $\Xi^{\pm}$ (bottom) p_T spectra measured in pp collisions at $\sqrt{s} = 13$ TeV in the V0M multiplicity class 0-100%. The values in parentheses refer to the toward-leading spectra and are reported only when a difference from the transverse-to-leading and full spectra is observed. No systematic uncertainty for the toward-leading $\Xi^{\pm}$ spectra is reported in the lowest p_T interval, as the measurement is performed for $p_T > 1.0(1.5)$ GeV/c, depending on the multiplicity class. No significant centre-of-mass energy dependence is observed. The three sources of uncertainty marked with an asterisk are observed to be partially uncorrelated across multiplicity, whereas all the other sources are fully correlated across multiplicity. See text for details.

JHEP09(2024)204

minimum bias pp collisions at $\sqrt{s} = 13$ TeV: the relative uncertainty decreases with p_{T} from about 2% down to $\sim 0.1\%$ for $p_{\mathrm{T}} > 4\,\mathrm{GeV}/c$. On the contrary, the variations are not significant for $\Xi^{\pm}$ toward-leading spectra. As for the choice of the $\Delta\eta$ region, this source does not affect the full yields.

The relative uncertainties associated with the topological selections and the choice of the $\Delta\eta$ and $\Delta\varphi$ intervals mildly depend on the multiplicity class.

Another systematic effect is related to the choice of the function used to fit the background of the invariant mass distributions of $\mathrm{K}^0_{\mathrm{S}}$ and $\Xi^{\pm}$ candidates. To quantify it, the fit to the background is performed with a second-degree polynomial and the invariant mass interval in which the fit is performed is varied. The results obtained in this way are compared with the default ones. For $\mathrm{K}^0_{\mathrm{S}}$, the relative systematic uncertainty increases with p_{T} up to 1.5%. For $\Xi^{\pm}$, the relative systematic uncertainty equals 0.5% in all p_{T} intervals. No dependence on the multiplicity class is observed.

To account for the simplified procedure applied to the subtraction of the contribution of misidentified $\Xi^{\pm}$ in the minimum bias samples, the $\Xi^{\pm}$ spectra measured in the 0–100% multiplicity class of pp collisions at $\sqrt{s} = 13$ TeV are compared with those obtained using the method based on the sidebands of the invariant mass distribution. The difference between the spectra obtained with the two methods is significant according to the Barlow criterion with a 2σ threshold in at least three p_{T} intervals, and their relative half-difference is assigned as a systematic uncertainty to the $\Xi^{\pm}$ spectra in all multiplicity classes in minimum bias events. The relative uncertainty decreases with increasing p_{T}, it is smaller than 1% for full and transverse-to-leading production and smaller than 3% for toward-leading production.

Since the $\mathrm{K}^0_{\mathrm{S}}$ efficiency depends on the multiplicity, a systematic uncertainty is assigned to $\mathrm{K}^0_{\mathrm{S}}$ spectra in order to account for possible differences between the multiplicity distribution in the data and in the Monte Carlo simulation used to compute the efficiency correction. To assess this uncertainty, the default $\mathrm{K}^0_{\mathrm{S}}$ efficiencies, computed using a Monte Carlo distribution based on Pythia8, are compared with those obtained using a different Monte Carlo simulation based on EPOS LHC [31], and a 1% uncertainty is added to account for the differences.

Another source of uncertainty for the $\Xi^{\pm}$ toward-leading spectra is related to the method applied to subtract the contribution of the underlying event in the low-p_{T} intervals ($p_{\mathrm{T}} < 2.5\,\mathrm{GeV}/c$) where the standard method cannot be applied due to large statistical uncertainties. To evaluate this uncertainty, the $\Xi^{\pm}$ toward-leading spectra are compared with those obtained using the standard procedure in the [2.0-2.5) GeV/c interval, where the number of $\Xi^{\pm}$ candidates is large enough to allow for the application of both methods. The systematic uncertainty, which amounts to 5–10% depending on the multiplicity class, is also assigned to the lower p_{T} intervals where the extraction procedure of the toward-leading yield differs from the standard one.

To take into account the imperfect reproduction of the detector material budget in the Monte Carlo simulation, the $\mathrm{K}^0_{\mathrm{S}}$ and $\Xi^{\pm}$ efficiencies are compared with those obtained using a Monte Carlo with a different dependence of the material budget on the radial distance from the interaction point. For $\mathrm{K}^0_{\mathrm{S}}$, the uncertainty associated with the material budget decreases with p_{T} from a maximum of 2% and shows a similar trend in all multiplicity classes. For $\Xi^{\pm}$, this systematic uncertainty amounts to 2% and is independent of multiplicity and p_{T}.

JHEP09(2024)204

The systematic uncertainties related to pileup rejection are inherited from the analysis of (multi-)strange hadron production in pp collisions at $\sqrt{s} = 13$ TeV [18]. To account for a residual contamination from in-bunch pileup, a relative systematic uncertainty of 2% is assigned to both K^0_S and $\Xi^\pm$ p_T spectra. The systematic uncertainty due to out-of-bunch pileup, evaluated in ref. [18] by changing the matching scheme of the decay tracks with the ITS and TOF detectors, amounts to 1.2% (2%) for K^0_S ($\Xi^\pm$) spectra in all p_T intervals and multiplicity classes.

Finally, another source of systematic uncertainty affecting the p_T-integrated yield is associated with choosing the fit function used to extrapolate the p_T-spectra. The uncertainty is given by the half-difference between the maximum and the minimum extrapolated yields obtained with the four different fit functions. This uncertainty amounts at most to 0.5% (4%) for full and transverse-to-leading yields of K^0_S ($\Xi^\pm$), and to 2% (4%) for toward-leading yields of K^0_S ($\Xi^\pm$).

Most of the sources of systematic uncertainties considered in this analysis are fully correlated across multiplicity, as they determine a shift of the yields in the same direction in all multiplicity classes. Three sources of uncertainty, namely the selections applied to identify K^0_S and $\Xi^\pm$ candidates and the choices of the $\Delta\varphi$ and $\Delta\eta$ intervals, are observed to be partially uncorrelated across multiplicity. For each of these sources, in order to determine the fraction of uncertainty which is uncorrelated across multiplicity, the ratio R^m_var is computed:

$$R^m_\mathrm{var} = \frac{y^m_\mathrm{var}/y^m_\mathrm{def}}{y^{0-100\%}_\mathrm{var}/y^{0-100\%}_\mathrm{def}}. \tag{3.2}$$

Here y^m_def and $y^{0-100\%}_\mathrm{def}$ are the default yields measured in a given p_T interval in the multiplicity class m and 0–100%, respectively, and y^m_var and $y^{0-100\%}_\mathrm{var}$ are the yields obtained by applying a systematic variation. If a source of uncertainty is fully correlated across multiplicity, $R^m_\mathrm{var} \sim 1$. For each source of systematic uncertainty, the uncorrelated relative uncertainty across multiplicity is computed as the maximum deviation of R^m_var from unity.

On average, the uncorrelated fraction of the total systematic uncertainty for K^0_S ($\Xi^\pm$) amounts to approximately 3%(5%), 10%(20%) and 25%(25%) for the full, transverse-to-leading and toward-leading production, respectively.

4 Results

The full, toward-leading and transverse-to-leading p_T distributions of K^0_S and $\Xi^\pm$ per unit $\Delta\eta\Delta\varphi$ area are shown for the different multiplicity classes in figures 3 and 4 for pp collisions at $\sqrt{s} = 13$ TeV and figures 5 and 6 for pp collisions at $\sqrt{s} = 5.02$ TeV. The bottom panels show the ratios to the spectra measured in the 0–100% multiplicity class. In all multiplicity classes and at both centre-of-mass energies, the toward-leading spectra (right panels) are harder, i.e. have a larger average p_T, than the transverse-to-leading (central panels) and full (left panels) spectra, as expected from the fact that the production in the direction of the trigger particle is associated with hard scattering processes. As shown in the bottom panels of figures 3–6, the transverse-to-leading and full p_T spectra increase with multiplicity in all p_T intervals, becoming harder as the multiplicity increases. This behaviour was already reported for strange hadron spectra measured inclusively, i.e. in all events, in Pb–Pb [11],

JHEP09(2024)204

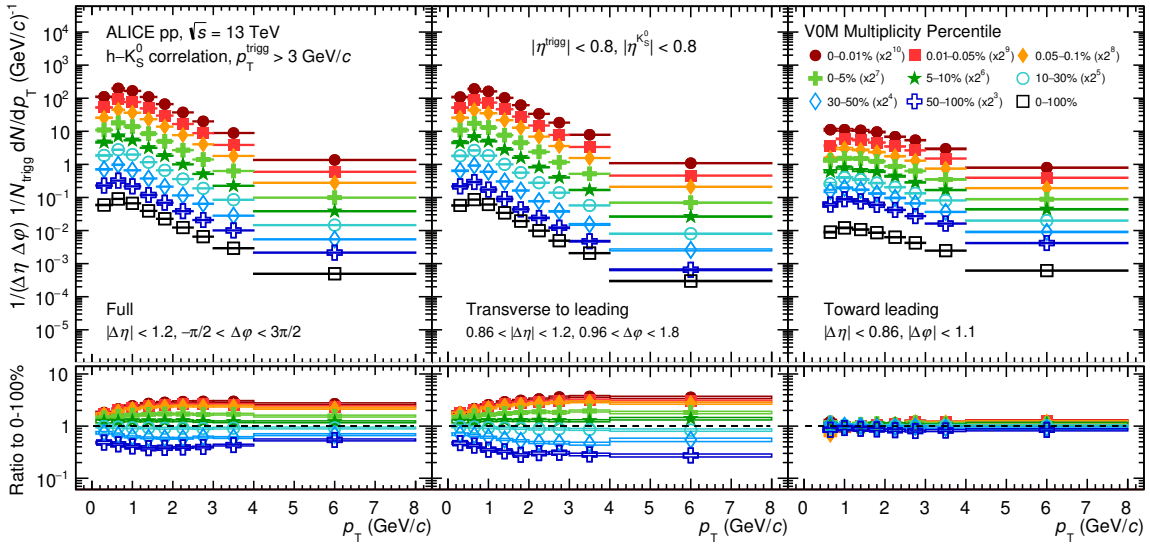

Figure 3. Transverse momentum distributions of K^0_S per unit $\Delta\eta\Delta\varphi$ area in pp collisions at $\sqrt{s} = 13$ TeV. The left, central and right panels refer to full, transverse-to-leading and toward-leading production, respectively. Different colours refer to different multiplicity classes selected using the V0 detector, as indicated in the legend. The spectra are scaled by different factors to improve the visibility. The bottom panels display the ratios to the spectra measured in the 0–100% multiplicity class. The statistical errors are represented by the error bars, the systematic uncertainties by the empty boxes. Error bars are smaller than the marker size and are therefore not visible.

p–Pb [12] and pp collisions [16, 18]. In Pb–Pb collisions this behaviour is more pronounced than in small collision systems and is interpreted as an indication of the presence of radial flow. In contrast to the full and transverse-to-leading spectra, the toward-leading spectra show a much smaller dependence on the multiplicity.

The full, transverse-to-leading and toward-leading p_T-integrated yields of K^0_S ($\Xi^\pm$) per unit $\Delta\eta\Delta\varphi$ area are shown in figure 7 (8) as a function of the charged-particle multiplicity measured at midrapidity in events with a trigger particle $\langle dN_{ch}/d\eta\rangle_{|\eta|<0.5,\ p_{T,trigg}>3\ GeV/c}$, in the following abbreviated with $\langle dN/d\eta\rangle_{trigg}$. The yields show no dependence on the centre-of-mass energy, as observed in previously published results [18]. The full and transverse-to-leading yields of both K^0_S and $\Xi^\pm$ increase with multiplicity faster than the toward-leading yields. For better visibility, the toward-leading p_T-integrated yields of K^0_S and $\Xi^\pm$ per unit $\Delta\eta\Delta\varphi$ area are separately shown in figure 9, where the $\Xi^\pm$ yields are scaled such that the lowest-multiplicity $\Xi^\pm$ yield matches the K^0_S one. Both the K^0_S and $\Xi^\pm$ yields are not compatible with a flat trend with multiplicity with a 5σ confidence level. The relative increase of the K^0_S yield from the lowest to the highest multiplicity is (1.22 ± 0.04), where the uncertainty is given by the sum in quadrature of the statistical and the systematic uncertainty uncorrelated in multiplicity. The relative increase of the $\Xi^\pm$ yield (1.93 ± 0.17) is significantly larger than the K^0_S one.

The yields are compared with the predictions of three different phenomenological models, namely Pythia8.2 with the Monash 2013 tune [41], Pythia8.2 with ropes [28] and EPOS LHC [31]. Pythia is based on the Lund string hadronisation model [54]. As shown in ref. [22], Pythia8.2 with the Monash 2013 tune cannot describe the strangeness enhancement with

JHEP09(2024)204

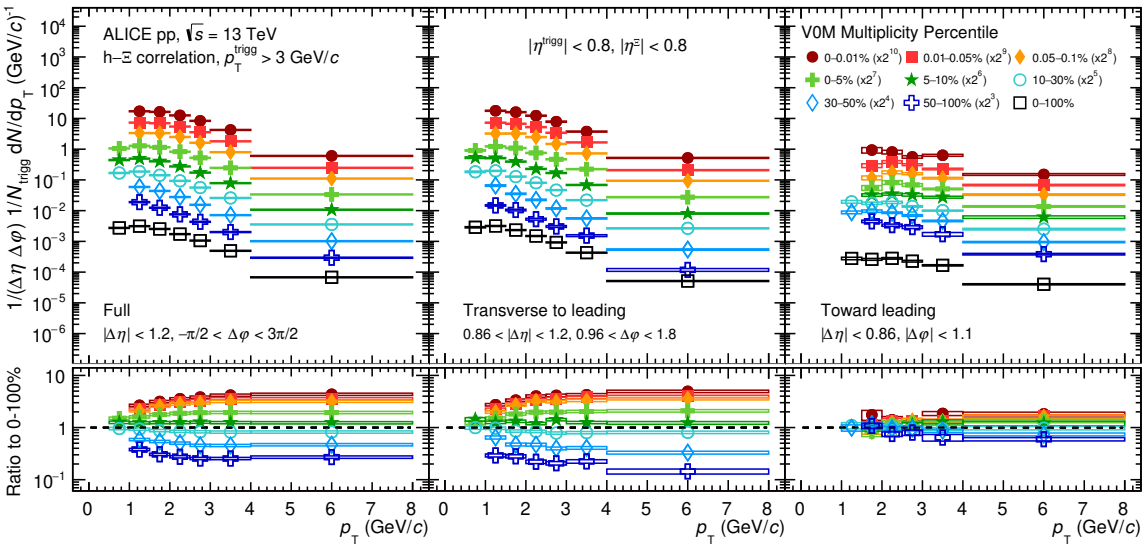

Figure 4. Transverse momentum distributions of $\Xi^{\pm}$ per unit $\Delta\eta\Delta\varphi$ area in pp collisions at $\sqrt{s} = 13$ TeV. The left, central and right panels refer to full, transverse-to-leading and toward-leading production, respectively. Different colours refer to different multiplicity classes selected using the V0 detector, as indicated in the legend. The spectra are scaled by different factors to improve the visibility. The bottom panels display the ratios to the spectra measured in the 0–100% multiplicity class. The statistical errors are represented by the error bars, the systematic uncertainties by the empty boxes. Error bars are smaller than the marker size and are therefore not visible.

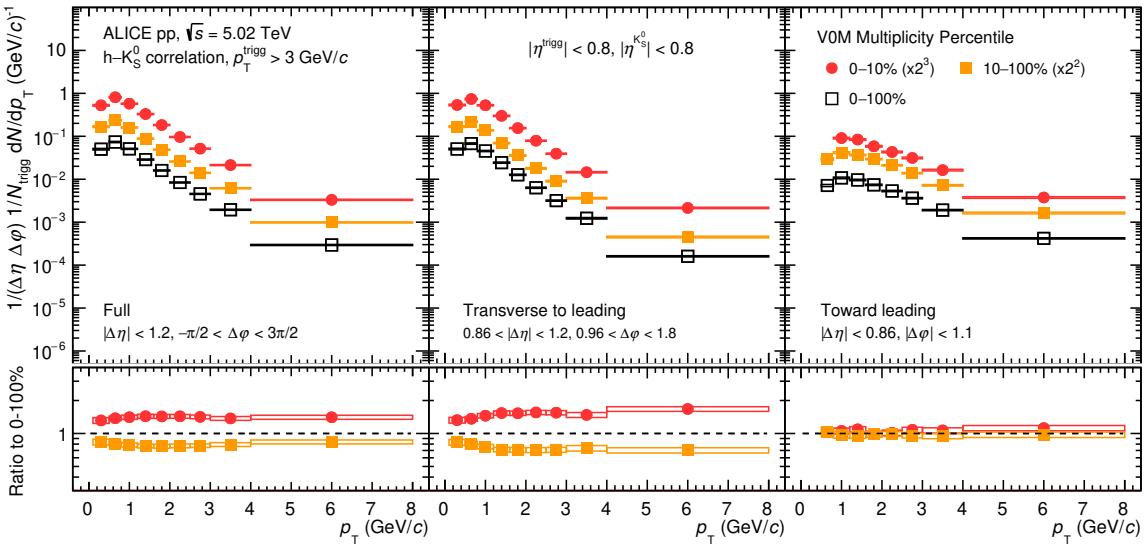

Figure 5. Transverse momentum distributions of K^0_S per unit $\Delta\eta\Delta\varphi$ area in pp collisions at $\sqrt{s} = 5.02$ TeV. The left, central and right panels refer to full, transverse-to-leading and toward-leading production, respectively. Different colours refer to different multiplicity classes selected using the V0 detector, as indicated in the legend. The spectra are scaled by different factors to improve the visibility. The bottom panels display the ratios to the spectra measured in the 0–100% multiplicity class. The statistical errors are represented by the error bars, the systematic uncertainties by the empty boxes. Error bars are smaller than the marker size and are therefore not visible.

JHEP09(2024)204

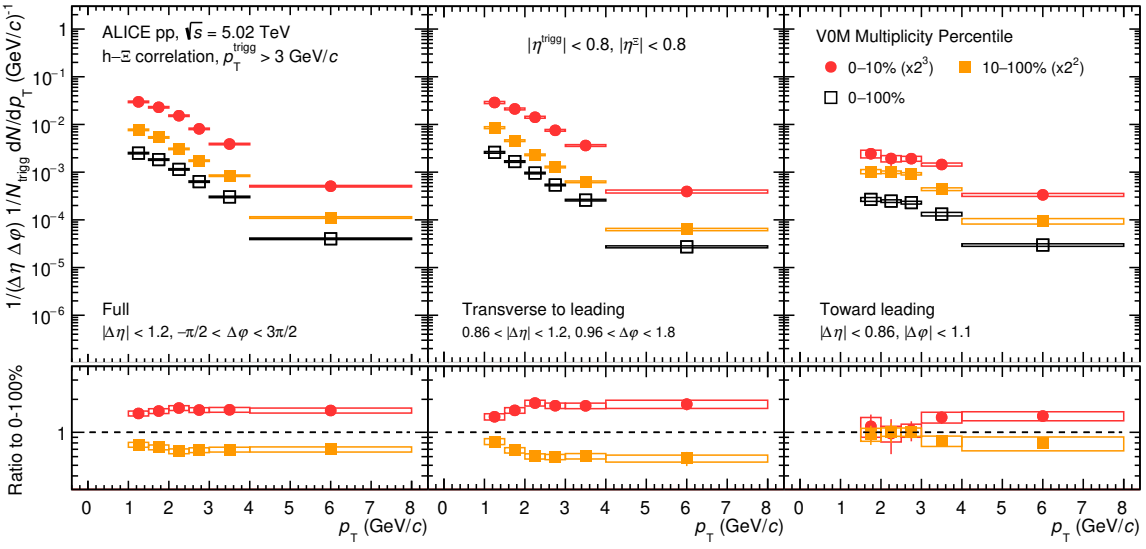

Figure 6. Transverse momentum distributions of $\Xi^{\pm}$ per unit $\Delta\eta\Delta\varphi$ area in pp collisions at $\sqrt{s} = 5.02$ TeV. The left, central and right panels refer to full, transverse-to-leading and toward-leading production, respectively. Different colours refer to different multiplicity classes selected using the V0 detector, as indicated in the legend. The spectra are scaled by different factors to improve the visibility. The bottom panels display the ratios to the spectra measured in the 0–100% multiplicity class. The statistical errors are represented by the error bars, the systematic uncertainties by the empty boxes. Error bars are smaller than the marker size and are therefore not visible.

multiplicity in INEL > 0 pp collisions: it underestimates the ratios between strange hadron and pion yields and does not reproduce their increase with multiplicity. The description is improved if overlapping strings are allowed to interact with each other, forming the so-called "colour ropes" [28]. Indeed, Pythia8 with colour ropes can qualitatively describe the strangeness enhancement with multiplicity in pp collisions, as shown in ref. [22]. Finally, the EPOS LHC [31] event generator implements the core-corona model [55], according to which strings in a low-density area form the corona and hadronise normally, while strings in a high-density area form the core and undergo collective hadronisation. As shown in ref. [15], EPOS LHC can reasonably well describe the K^0_S/π ratio measured in INEL > 0 pp collisions, while it overestimates the strangeness enhancement with multiplicity for the Λ, $\Xi^{\pm}$ and $\Omega^{\pm}$ baryons.

The bottom panels of figures 7–8–9 display the ratios between the model predictions and the cubic splines fitted to the data points. Three sources of systematic uncertainty affecting the model predictions were considered: the choice of $\Delta\eta$ and $\Delta\varphi$ regions, which is evaluated as described in section 3.5 for the data and is found not to be significant according to the Barlow criterion for both the toward-leading and the transverse-to-leading production, and the extrapolation of the yields in the unmeasured p_T regions: $p_T < 0.5(1.0)$ GeV/c for K^0_S ($\Xi^{\pm}$) toward-leading yield and $p_T < 0.5$ GeV/c for $\Xi^{\pm}$ full and transverse-to-leading yields. All the models underestimate the full and the transverse-to-leading K^0_S yields (figure 7). The underestimation is more significant at low multiplicity ($\langle dN/d\eta\rangle_{trigg} \sim 10$), where all models underestimate the yields by about 30%. At high multiplicity ($\langle dN/d\eta\rangle_{trigg} \sim 30$), both Pythia8 implementations underestimate the yields by about 15%, while EPOS LHC

JHEP09(2024)204

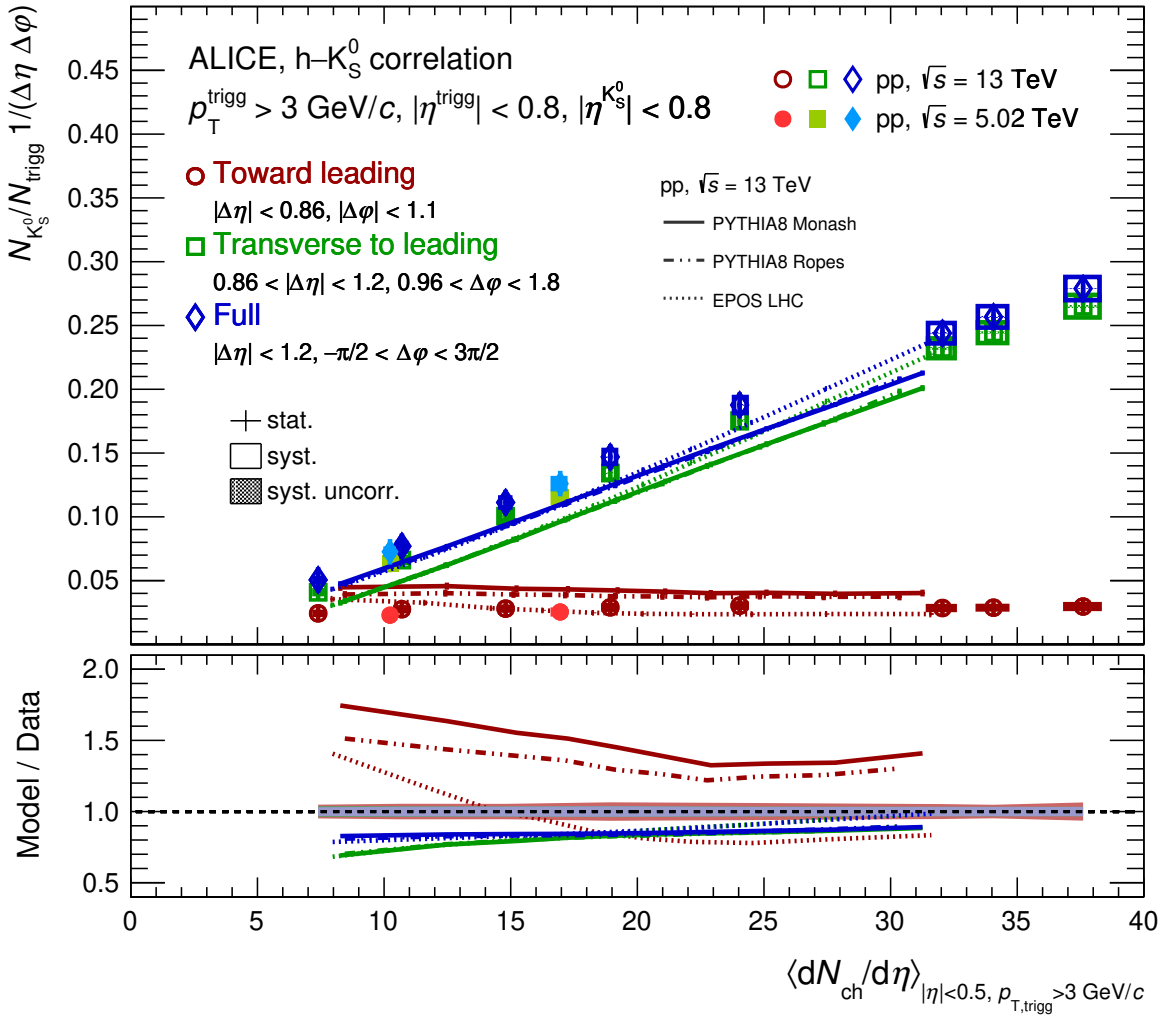

Figure 7. Upper panel: full (blue), transverse-to-leading (green) and toward-leading (red) K^0_S yields per unit $\Delta\eta\Delta\varphi$ area as a function of the charged-particle multiplicity measured in events with a trigger particle. The data points are drawn with markers, the model predictions with lines of different styles, as indicated in the legend. Statistical and systematic uncertainties of the data points are shown by error bars and empty boxes, respectively. Shadowed boxes represent systematic uncertainties uncorrelated across multiplicity. The sum in quadrature of statistical and systematic uncertainties of the model predictions are shown by error bars, too small to be visible in the plot. Bottom panel: ratio between the model predictions and the cubic spline fitted to the data points. The shaded band around one represents the sum in quadrature of the statistical and systematic uncertainties of the data points.

predicts values compatible with the measured ones. The increase with multiplicity of the toward-leading yield of K^0_S (figure 9) is not reproduced by any of the three models: both Pythia8 implementations overestimate the yields and show a hint of decrease with multiplicity, whereas EPOS LHC predicts a decrease of the toward-leading yield with multiplicity. The deviation of the models from the full and transverse-to-leading $\Xi^{\pm}$ yields (figure 8) is larger than the deviation from those of the K^0_S (figure 7). Both Pythia8 implementations underestimate the yields: Pythia8 Monash underestimates them by approximately 70% over

JHEP09(2024)204

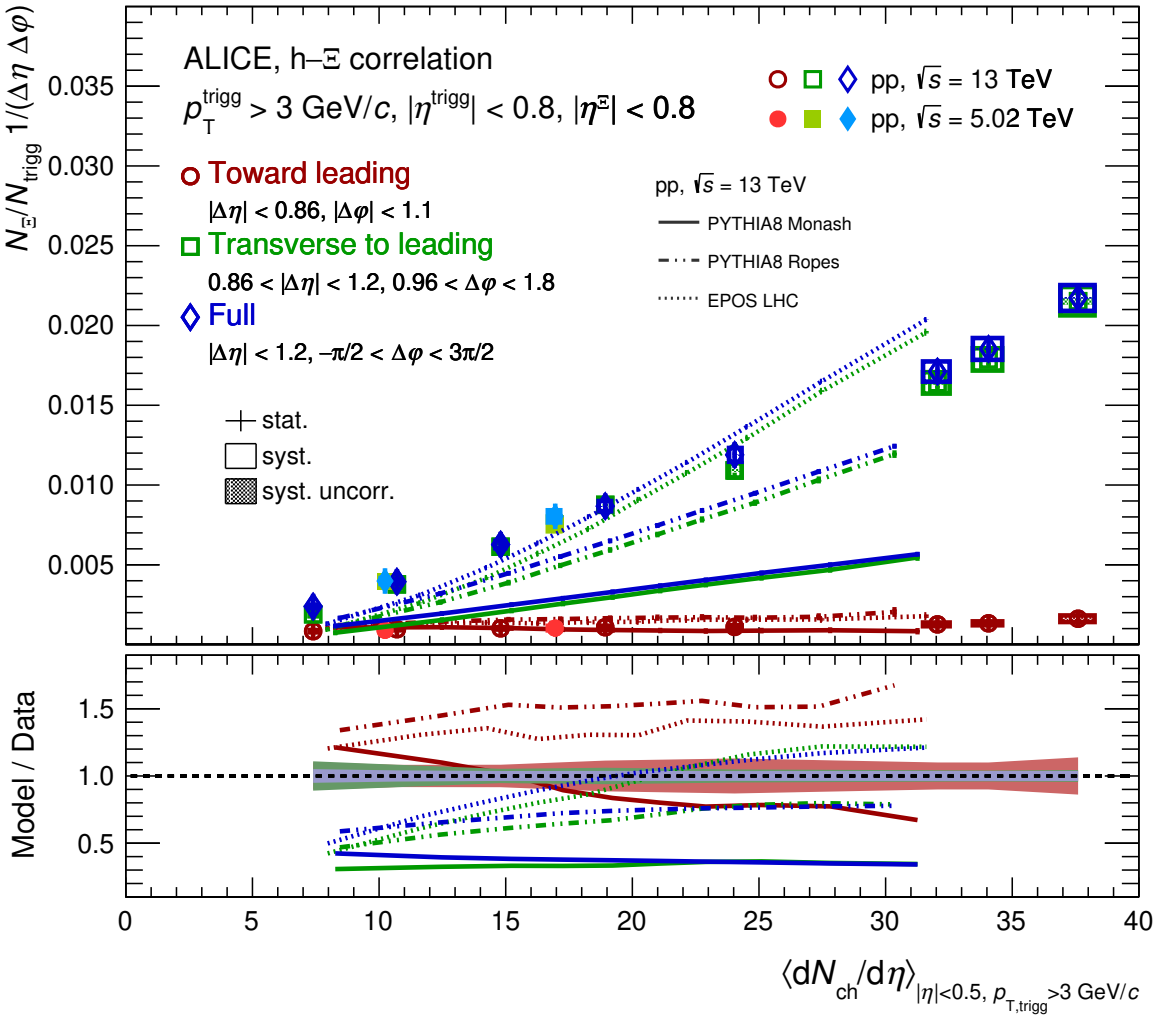

Figure 8. Upper panel: full (blue), transverse-to-leading (green) and toward-leading (red) $\Xi^{\pm}$ yields per unit $\Delta\eta\Delta\varphi$ area as a function of the charged-particle multiplicity measured in events with a trigger particle. The data points are drawn with markers, the model predictions with lines of different styles, as indicated in the legend. Statistical and systematic uncertainties of the data points are shown by error bars and empty boxes, respectively. Shadowed boxes represent systematic uncertainties uncorrelated across multiplicity. The sum in quadrature of statistical and systematic uncertainties of the model predictions are shown by error bars, too small to be visible in the plot. Bottom panel: ratio between the model predictions and the cubic spline fitted to the data points. The shaded band around one represents the sum in quadrature of the statistical and systematic uncertainties of the data points.

the whole multiplicity interval, whereas Pythia8 with ropes underestimates them by about 50% at low multiplicity and 20% at high multiplicity. EPOS LHC underestimates the yield at low multiplicity by about 50% and overestimates it by about 20% at high multiplicity, predicting an increase of the transverse-to-leading and full yields with multiplicity larger than the one observed in the data. The increase with multiplicity of the $\Xi^{\pm}$ toward-leading yield (figure 9) is not described by Pythia8 Monash, which predicts a nearly flat trend with multiplicity. On the contrary, Pythia8 with ropes and EPOS LHC can qualitatively

JHEP09(2024)204

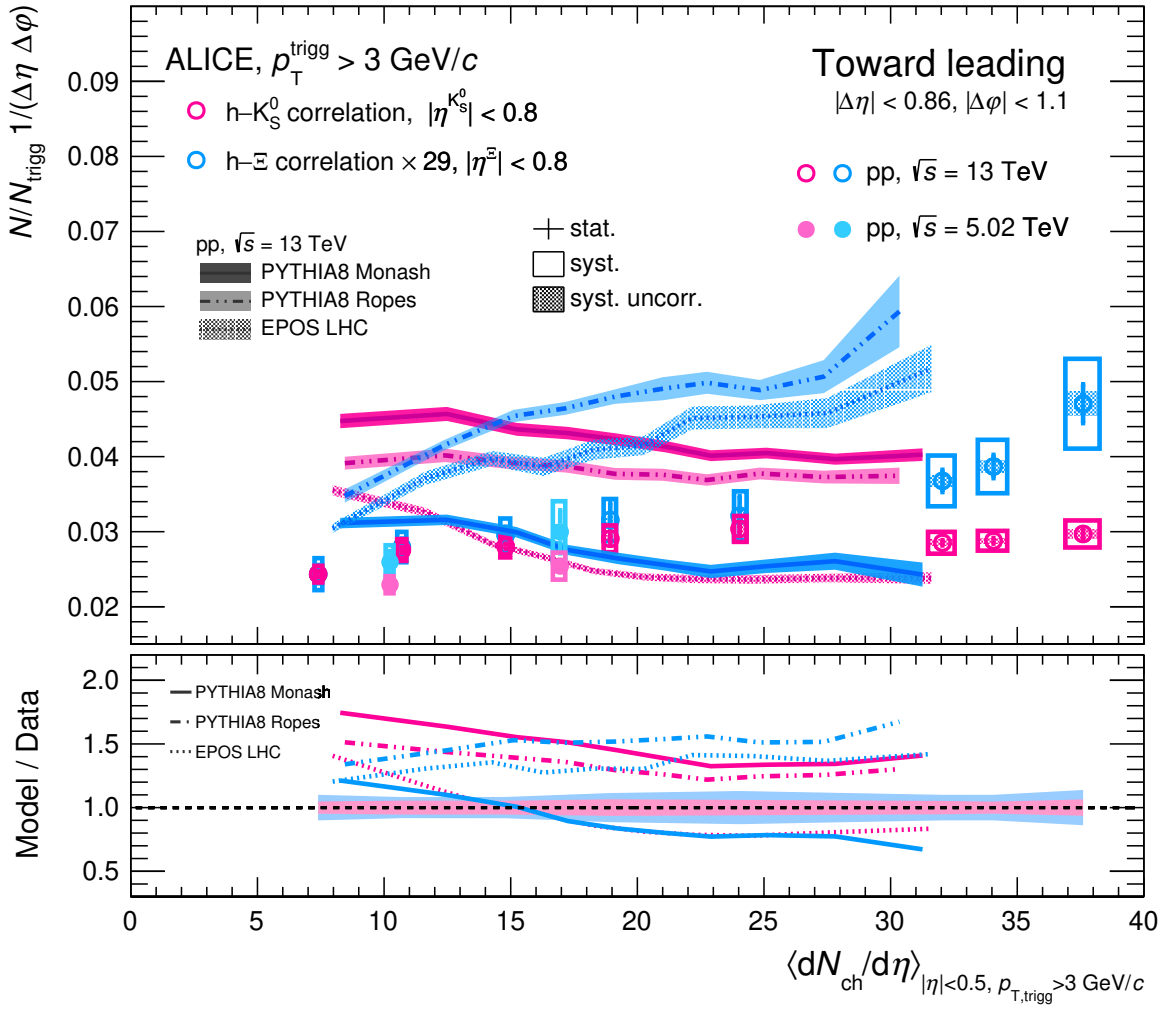

Figure 9. Upper panel: toward-leading K^0_S (magenta) and $\Xi^{\pm}$ (light blue) yields per unit $\Delta\eta\Delta\varphi$ area as a function of the charged-particle multiplicity measured in events with a trigger particle. The $\Xi^{\pm}$ yields are scaled such that the lowest-multiplicity $\Xi^{\pm}$ yield matches the K^0_S one. The data points are drawn with markers, the model predictions with lines of different styles, as indicated in the legend. Statistical and systematic uncertainties of the data points are shown by error bars and empty boxes, respectively. Shadowed boxes represent systematic uncertainties uncorrelated across multiplicity. The width of the bands represents the sum in quadrature of statistical and systematic uncertainties of the model predictions. Bottom panel: ratio between the model predictions and the cubic spline fitted to the data points. The shaded band around one represents the sum in quadrature of the statistical and systematic uncertainties of the data points.

JHEP09(2024)204

reproduce the increasing trend. These models, however, overestimate the toward-leading yields over the whole multiplicity interval.

The ratios between $\Xi^{\pm}$ and K^0_S yields as a function of $\langle \mathrm{d}N/\mathrm{d}\eta \rangle_{\mathrm{trigg}}$ are shown in the top panel of figure 10, together with the model predictions. In the data, the ratio of full yields increases with multiplicity: this could be related to the larger strangeness content of the $\Xi^{\pm}$ with respect to the K^0_S. Indeed, the enhanced production of strange hadrons with increasing multiplicity was observed to be higher for particles with larger strangeness content [15]. The ratio of transverse-to-leading yields increases with the multiplicity by a factor (1.75 ± 0.16), with the error given by the sum in quadrature of the statistical and systematic uncertainty uncorrelated across multiplicity. It is compatible with the ratio of full yields, because the full yield is dominated by transverse-to-leading production, as shown in figures 7 and 8. Also the toward-leading ratio increases with multiplicity: a flat behaviour with multiplicity is excluded since a zero-degree polynomial is not able to describe the ratio within the uncertainties uncorrelated across multiplicity. The increase of the toward-leading ratio from the lowest to the highest multiplicity interval equals a factor (1.58 ± 0.15). As shown by the double ratio between the toward-leading and the transverse-to-leading $\Xi^{\pm}/\mathrm{K}^0_\mathrm{S}$ ratios displayed in the bottom panel of figure 10, the toward-leading ratio is approximately 40% smaller than the transverse-to-leading ratio, suggesting that the production of $\Xi^{\pm}$ with respect to K^0_S is favoured in transverse-to-leading processes over the whole multiplicity interval where the measurement was performed. The double ratio is well described by a zero-degree polynomial with a $\chi^2/\mathrm{ndf} = 6.6/7$, indicating that the transverse-to-leading and toward-leading yield ratios increase with multiplicity in a similar way.

The central panel of figure 10 displays the ratio between the model predictions and the data points. Pythia8 Monash underestimates the ratios in the whole multiplicity interval, due to the large underestimation of the full and transverse-to-leading $\Xi^{\pm}$ yields and of the overestimation of the K^0_S toward-leading yield. The toward-leading ratio does not describe the increase observed in the data. The full and transverse-to-leading ratios show instead an increase with multiplicity, which is smaller than the one observed in the data, as suggested by the decrease of the model over data ratio from about 0.5 at low multiplicity to about 0.4 at high multiplicity. Pythia8 with ropes can qualitatively describe the increase of the ratios with multiplicity observed in the data. However, the full and transverse-to-leading ratios are underestimated in the whole multiplicity interval, and particularly at low multiplicity, where the underestimation of the $\Xi^{\pm}$ yields is larger. The toward-leading ratio is in qualitative agreement with the data, but its increase with multiplicity is slightly overestimated: this fair agreement is resulting from the overestimation of both the K^0_S and the $\Xi^{\pm}$ toward-leading yields. Finally, EPOS LHC overestimates the increase with multiplicity of the full and transverse-to-leading ratios, as a consequence of the overestimation of the increase with multiplicity of $\Xi^{\pm}$ yields. In particular, the full and transverse-to-leading ratios are underestimated by about 30% at low multiplicity and overestimated by about 20% at high multiplicity. The toward-leading ratio is instead overestimated in the whole multiplicity interval, mainly as a consequence of the overestimation of the $\Xi^{\pm}$ toward-leading yield. Moreover, its increase with multiplicity is larger than the one observed in the data because the K^0_S toward-leading yields predicted by EPOS LHC decrease with multiplicity. As shown in the bottom panel of figure 10,

JHEP09(2024)204

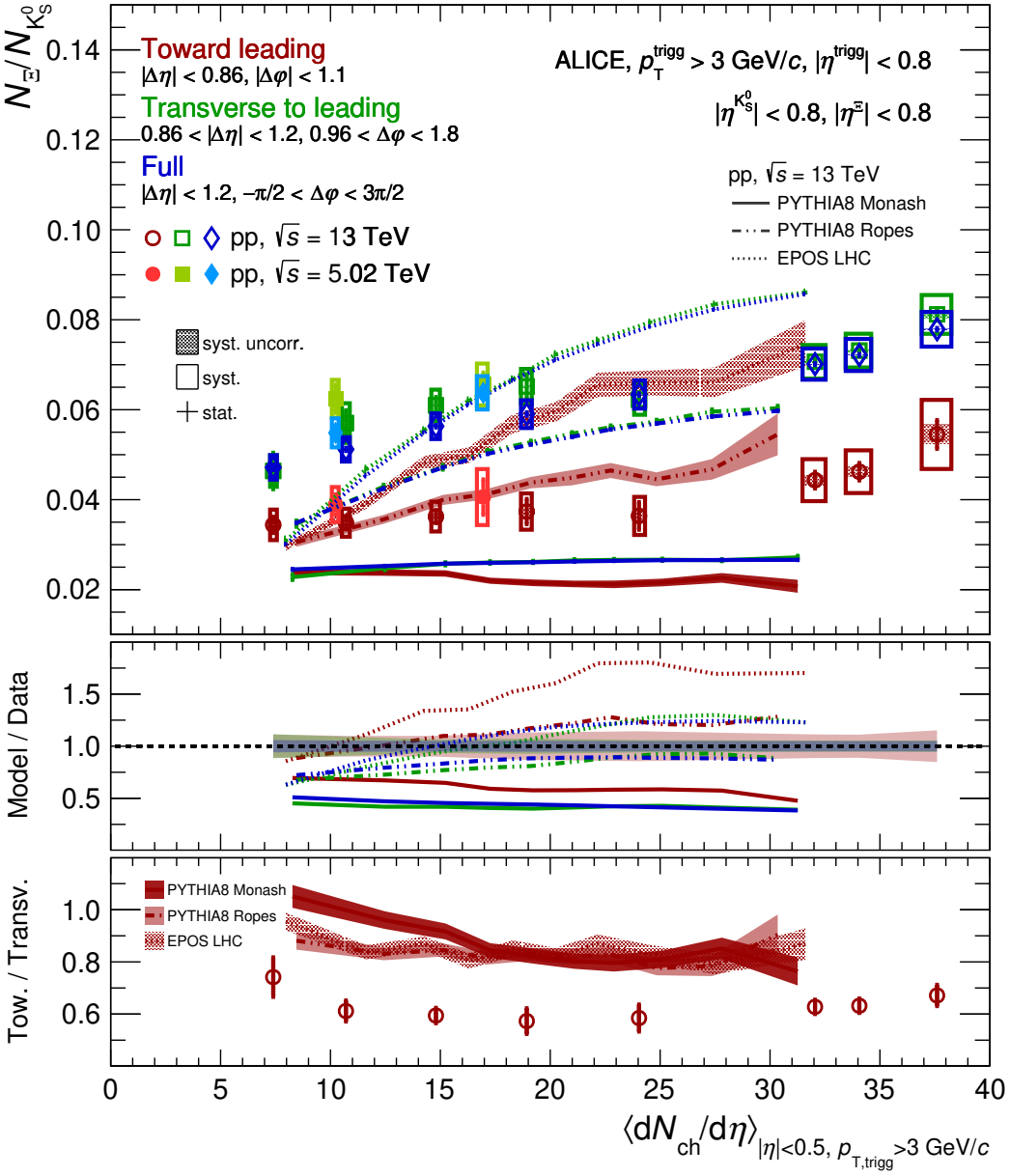

Figure 10. Top panel: full (blue), transverse-to-leading (green) and toward-leading (red) $\Xi^{\pm}/\mathrm{K}^0_\mathrm{S}$ yield ratios as a function of the charged-particle multiplicity measured at midrapidity in events with a trigger particle. The data points are drawn with markers, and their statistical and systematic uncertainties are shown by error bars and empty boxes, respectively. Shadowed boxes represent systematic uncertainties uncorrelated across multiplicity. The model predictions are drawn with lines of different styles. The width of the bands represents the sum in quadrature of statistical and systematic uncertainties of the model predictions, and is visible only for toward-leading production. Central panel: ratio between the model predictions and the cubic spline fitted to the data points. The shaded band around unity represents the sum in quadrature of the statistical and systematic uncertainties of the data points. Bottom panel: double ratio between the toward-leading and the transverse-to-leading $\Xi^{\pm}/\mathrm{K}^0_\mathrm{S}$ ratios.

JHEP09(2024)204

the three models predict a larger double ratio than the one measured in the data, i.e. they overestimate the toward-leading $\Xi^{\pm}/\mathrm{K}^0_\mathrm{S}$ production with respect to the transverse-to-leading one. The double ratios predicted by Pythia8 with ropes and EPOS LHC are smaller than unity and can be described with a zero-degree polynomial. On the contrary, the double ratio predicted by Pythia8 Monash is compatible with one in the lowest multiplicity class and decreases to about 0.8 in the highest multiplicity class.

The comparison of the Monte Carlo model predictions with the data suggests that none of the considered models describes strange hadron production in hard scattering processes or in the underlying event.

5 Summary and outlook

The production of K^0_S and $\Xi^{\pm}$ in pp collisions at $\sqrt{s} = 5.02$ TeV and at $\sqrt{s} = 13$ TeV was measured in the direction of the highest-p_T charged particle (trigger particle) and in the direction transverse to it. The toward-leading p_T spectra are harder than the transverse-to-leading ones, as expected from the fact that the production in the direction of the trigger particle is associated with hard scattering processes, whereas the production in the transverse-to-leading direction is related to the underlying event.

The full p_T-integrated yields per unit $\Delta\eta\Delta\varphi$ of K^0_S and $\Xi^{\pm}$ are dominated by transverse-to-leading production and increase with the multiplicity of charged particles produced at midrapidity. The toward-leading yields show instead a milder dependence on the multiplicity, indicating that the contribution of transverse-to-leading processes relative to toward-leading ones increases with the multiplicity. The K^0_S and $\Xi^{\pm}$ yields do not show any significant centre-of-mass energy dependence.

The ratio between the $\Xi^{\pm}$ and the K^0_S yields provides insight into the strangeness enhancement effect, since the strangeness content of the $\Xi^{\pm}$ ($|S|$=2) is larger than the K^0_S one ($|S|$=1). Both the transverse-to-leading and the toward-leading $\Xi^{\pm}/\mathrm{K}^0_\mathrm{S}$ yield ratios increase with the multiplicity of charged particles. The transverse-to-leading ratio is larger than the toward-leading one, suggesting that the relative production of $\Xi^{\pm}$ with respect to K^0_S is favoured in underlying event processes.

None of the considered models, namely Pythia8 Monash tune, Pythia8 with ropes and EPOS LHC, can quantitatively describe the transverse-to-leading and toward-leading yields of K^0_S and $\Xi^{\pm}$. Both Pythia8 implementations underestimate the full and the transverse-to-leading K^0_S and $\Xi^{\pm}$ yields, with the largest underestimation observed for the $\Xi^{\pm}$ yields. The increase of the full and transverse-to-leading $\Xi^{\pm}$ yields with multiplicity is overestimated by both Pythia8 with ropes and EPOS LHC, leading to an overestimation of the increase of the full and transverse-to-leading $\Xi^{\pm}/\mathrm{K}^0_\mathrm{S}$ yield ratios with multiplicity. The increase of the toward-leading yield of K^0_S with multiplicity is not reproduced by any of the three models. On the contrary, the increase of the $\Xi^{\pm}$ toward-leading yield with multiplicity is qualitatively reproduced by Pythia8 with ropes and EPOS LHC, while Pythia8 Monash predicts a flat trend with multiplicity. Overall, the comparison with the data indicates that the strange hadron production associated with both hard scattering processes and the underlying event is not properly described by any of the considered models. Additionally,

JHEP09(2024)204

other models such as the most recent implementation of the core-corona approach EPOS4 [56] could be tested.

Further investigation of the origin of the enhanced production of strange hadrons in high-multiplicity pp collisions with respect to low-multiplicity ones will be possible thanks to the huge sample of pp collisions that is being collected during the ongoing Run 3, which is expected to be three orders of magnitude larger than the Run 2 one. With Run 3 data, measuring the toward-leading and transverse-to-leading yields of the triple-strange baryon $\Omega^{\pm}$ as a function of the charged-particle multiplicity will become feasible. Additionally, it will be possible to study the dependence of the toward-leading and transverse-to-leading $\Xi^{\pm}$ yields on the minimum p_{T} of the trigger particle, with higher p_{T} thresholds reducing the contamination from particles not originating from hard-scattering events. These studies will help improve the current understanding of strange hadron production mechanisms.

Acknowledgments

The ALICE Collaboration would like to thank all its engineers and technicians for their invaluable contributions to the construction of the experiment and the CERN accelerator teams for the outstanding performance of the LHC complex. The ALICE Collaboration gratefully acknowledges the resources and support provided by all Grid centres and the Worldwide LHC Computing Grid (WLCG) collaboration. The ALICE Collaboration acknowledges the following funding agencies for their support in building and running the ALICE detector: A. I. Alikhanyan National Science Laboratory (Yerevan Physics Institute) Foundation (ANSL), State Committee of Science and World Federation of Scientists (WFS), Armenia; Austrian Academy of Sciences, Austrian Science Fund (FWF): [M 2467-N36] and Nationalstiftung für Forschung, Technologie und Entwicklung, Austria; Ministry of Communications and High Technologies, National Nuclear Research Center, Azerbaijan; Conselho Nacional de Desenvolvimento Científico e Tecnológico (CNPq), Financiadora de Estudos e Projetos (Finep), Fundação de Amparo à Pesquisa do Estado de São Paulo (FAPESP) and Universidade Federal do Rio Grande do Sul (UFRGS), Brazil; Bulgarian Ministry of Education and Science, within the National Roadmap for Research Infrastructures 2020-2027 (object CERN), Bulgaria; Ministry of Education of China (MOEC) , Ministry of Science & Technology of China (MSTC) and National Natural Science Foundation of China (NSFC), China; Ministry of Science and Education and Croatian Science Foundation, Croatia; Centro de Aplicaciones Tecnológicas y Desarrollo Nuclear (CEADEN), Cubaenergía, Cuba; Ministry of Education, Youth and Sports of the Czech Republic, Czech Republic; The Danish Council for Independent Research | Natural Sciences, the VILLUM FONDEN and Danish National Research Foundation (DNRF), Denmark; Helsinki Institute of Physics (HIP), Finland; Commissariat à l'Energie Atomique (CEA) and Institut National de Physique Nucléaire et de Physique des Particules (IN2P3) and Centre National de la Recherche Scientifique (CNRS), France; Bundesministerium für Bildung und Forschung (BMBF) and GSI Helmholtzzentrum für Schwerionenforschung GmbH, Germany; General Secretariat for Research and Technology, Ministry of Education, Research and Religions, Greece; National Research, Development and Innovation Office, Hungary; Department of Atomic Energy Government of India (DAE), Department of Science and Technology, Government of India (DST), University Grants Commission, Government of India

JHEP09(2024)204

(UGC) and Council of Scientific and Industrial Research (CSIR), India; National Research and Innovation Agency - BRIN, Indonesia; Istituto Nazionale di Fisica Nucleare (INFN), Italy; Japanese Ministry of Education, Culture, Sports, Science and Technology (MEXT) and Japan Society for the Promotion of Science (JSPS) KAKENHI, Japan; Consejo Nacional de Ciencia (CONACYT) y Tecnología, through Fondo de Cooperación Internacional en Ciencia y Tecnología (FONCICYT) and Dirección General de Asuntos del Personal Academico (DGAPA), Mexico; Nederlandse Organisatie voor Wetenschappelijk Onderzoek (NWO), Netherlands; The Research Council of Norway, Norway; Pontificia Universidad Católica del Perú, Peru; Ministry of Science and Higher Education, National Science Centre and WUT ID-UB, Poland; Korea Institute of Science and Technology Information and National Research Foundation of Korea (NRF), Republic of Korea; Ministry of Education and Scientific Research, Institute of Atomic Physics, Ministry of Research and Innovation and Institute of Atomic Physics and Universitatea Nationala de Stiinta si Tehnologie Politehnica Bucuresti, Romania; Ministry of Education, Science, Research and Sport of the Slovak Republic, Slovakia; National Research Foundation of South Africa, South Africa; Swedish Research Council (VR) and Knut & Alice Wallenberg Foundation (KAW), Sweden; European Organization for Nuclear Research, Switzerland; Suranaree University of Technology (SUT), National Science and Technology Development Agency (NSTDA) and National Science, Research and Innovation Fund (NSRF via PMU-B B05F650021), Thailand; Turkish Energy, Nuclear and Mineral Research Agency (TENMAK), Turkey; National Academy of Sciences of Ukraine, Ukraine; Science and Technology Facilities Council (STFC), United Kingdom; National Science Foundation of the United States of America (NSF) and United States Department of Energy, Office of Nuclear Physics (DOE NP), United States of America. In addition, individual groups or members have received support from: Czech Science Foundation (grant no. 23-07499S), Czech Republic; European Research Council (grant no. 950692), European Union; ICSC - Centro Nazionale di Ricerca in High Performance Computing, Big Data and Quantum Computing, European Union - NextGenerationEU; Academy of Finland (Center of Excellence in Quark Matter) (grant nos. 346327, 346328), Finland.

Open Access. This article is distributed under the terms of the Creative Commons Attribution License (CC-BY4.0), which permits any use, distribution and reproduction in any medium, provided the original author(s) and source are credited.

References

[1] J. Rafelski and B. Muller, *Strangeness Production in the Quark-Gluon Plasma*, *Phys. Rev. Lett.* **48** (1982) 1066 [*Erratum ibid.* **56** (1986) 2334] [INSPIRE].

[2] P. Koch, J. Rafelski and W. Greiner, *Strange hadrons in hot nuclear matter*, *Phys. Lett. B* **123** (1983) 151 [INSPIRE].

[3] P. Koch, B. Muller and J. Rafelski, *Strangeness in relativistic heavy ion collisions*, *Phys. Rept.* **142** (1986) 167 [INSPIRE].

[4] NA35 collaboration, *Neutral strange particle production in sulphur-sulphur and proton-sulphur collisions at 200 GeV/nucleon*, *Z. Phys. C* **48** (1990) 191 [INSPIRE].

JHEP09(2024)204

[5] WA97 collaboration, *Strangeness enhancement at mid-rapidity in Pb–Pb collisions at 158 A GeV/c*, *Phys. Lett. B* **449** (1999) 401 [INSPIRE].

[6] NA57 collaboration, *Enhancement of hyperon production at central rapidity in 158 A GeV/c Pb–Pb collisions*, *J. Phys. G* **32** (2006) 427 [nucl-ex/0601021] [INSPIRE].

[7] NA49 collaboration, *Ω^- and $\overline{\Omega}^+$ production in central Pb + Pb collisions at 40 and 158A GeV*, *Phys. Rev. Lett.* **94** (2005) 192301 [nucl-ex/0409004] [INSPIRE].

[8] NA49 collaboration, *Energy dependence of Λ and Ξ production in central Pb–Pb collisions at 20A, 30A, 40A, 80A, and 158A GeV measured at the CERN Super Proton Synchrotron*, *Phys. Rev. C* **78** (2008) 034918 [arXiv:0804.3770] [INSPIRE].

[9] NA49 collaboration, *System-size dependence of Λ and Ξ production in nucleus-nucleus collisions at 40A and 158A GeV measured at the CERN Super Proton Synchrotron*, *Phys. Rev. C* **80** (2009) 034906 [arXiv:0906.0469] [INSPIRE].

[10] STAR collaboration, *Enhanced strange baryon production in Au + Au collisions compared to pp at $\sqrt{s_{\rm NN}}$ = 200 GeV*, *Phys. Rev. C* **77** (2008) 044908 [arXiv:0705.2511] [INSPIRE].

[11] ALICE collaboration, *Multi-strange baryon production at mid-rapidity in Pb-Pb collisions at $\sqrt{s_{NN}}$ = 2.76 TeV*, *Phys. Lett. B* **728** (2014) 216 [arXiv:1307.5543] [INSPIRE].

[12] ALICE collaboration, *Multi-strange baryon production in p–Pb collisions at $\sqrt{s_{\rm NN}}$ = 5.02 TeV*, *Phys. Lett. B* **758** (2016) 389 [arXiv:1512.07227] [INSPIRE].

[13] ALICE collaboration, *Multiplicity dependence of pion, kaon, proton and lambda production in p–Pb collisions at $\sqrt{s_{\rm NN}}$ = 5.02 TeV*, *Phys. Lett. B* **728** (2014) 25 [arXiv:1307.6796] [INSPIRE].

[14] CMS collaboration, *Strange hadron production in pp and pPb collisions at $\sqrt{s_{\rm NN}}$ = 5.02 TeV*, *Phys. Rev. C* **101** (2020) 064906 [arXiv:1910.04812] [INSPIRE].

[15] ALICE collaboration, *Enhanced production of multi-strange hadrons in high-multiplicity proton-proton collisions*, *Nature Phys.* **13** (2017) 535 [arXiv:1606.07424] [INSPIRE].

[16] ALICE collaboration, *Multiplicity dependence of light-flavor hadron production in pp collisions at $\sqrt{s}$ = 7 TeV*, *Phys. Rev. C* **99** (2019) 024906 [arXiv:1807.11321] [INSPIRE].

[17] ALICE collaboration, *Production of light-flavor hadrons in pp collisions at $\sqrt{s} = 7$ and $\sqrt{s} = 13$ TeV*, *Eur. Phys. J. C* **81** (2021) 256 [arXiv:2005.11120] [INSPIRE].

[18] ALICE collaboration, *Multiplicity dependence of (multi-)strange hadron production in proton-proton collisions at $\sqrt{s} = 13$ TeV*, *Eur. Phys. J. C* **80** (2020) 167 [arXiv:1908.01861] [INSPIRE].

[19] LHCb collaboration, *Prompt K^0_s production in pp collisions at $\sqrt{s} = 0.9$ TeV*, *Phys. Lett. B* **693** (2010) 69 [arXiv:1008.3105] [INSPIRE].

[20] CMS collaboration, *Strange particle production in pp collisions at $\sqrt{s} = 0.9$ and 7 TeV*, *JHEP* **05** (2011) 064 [arXiv:1102.4282] [INSPIRE].

[21] ATLAS collaboration, *K^0_S and Λ production in pp interactions at $\sqrt{s} = 0.9$ and 7 TeV measured with the ATLAS detector at the LHC*, *Phys. Rev. D* **85** (2012) 012001 [arXiv:1111.1297] [INSPIRE].

[22] ALICE collaboration, *Multiplicity dependence of π, K, and p production in pp collisions at $\sqrt{s} = 13$ TeV*, *Eur. Phys. J. C* **80** (2020) 693 [arXiv:2003.02394] [INSPIRE].

[23] ALICE collaboration, *Long- and short-range correlations and their event-scale dependence in high-multiplicity pp collisions at $\sqrt{s} = 13$ TeV*, *JHEP* **05** (2021) 290 [arXiv:2101.03110] [INSPIRE].

JHEP09(2024)204

[24] CMS collaboration, *Measurement of long-range near-side two-particle angular correlations in pp collisions at $\sqrt{s} = 13$ TeV*, *Phys. Rev. Lett.* **116** (2016) 172302 [arXiv:1510.03068] [INSPIRE].

[25] CMS collaboration, *Evidence for collectivity in pp collisions at the LHC*, *Phys. Lett. B* **765** (2017) 193 [arXiv:1606.06198] [INSPIRE].

[26] ATLAS collaboration, *Observation of Long-Range Elliptic Azimuthal Anisotropies in $\sqrt{s} = 13$ and 2.76 TeV pp Collisions with the ATLAS Detector*, *Phys. Rev. Lett.* **116** (2016) 172301 [arXiv:1509.04776] [INSPIRE].

[27] ALICE collaboration, *Multiplicity and event-scale dependent flow and jet fragmentation in pp collisions at $\sqrt{s} = 13$ TeV and in p–Pb collisions at $\sqrt{s_{NN}} = 5.02$ TeV*, *JHEP* **03** (2024) 092 [arXiv:2308.16591] [INSPIRE].

[28] C. Bierlich, G. Gustafson, L. Lönnblad and A. Tarasov, *Effects of overlapping strings in pp collisions*, *JHEP* **03** (2015) 148 [arXiv:1412.6259] [INSPIRE].

[29] M. Bahr et al., *Herwig++ physics and manual*, *Eur. Phys. J. C* **58** (2008) 639 [arXiv:0803.0883] [INSPIRE].

[30] J. Bellm et al., *Herwig 7.0/Herwig++ 3.0 release note*, *Eur. Phys. J. C* **76** (2016) 196 [arXiv:1512.01178] [INSPIRE].

[31] T. Pierog et al., *EPOS LHC: Test of collective hadronization with data measured at the CERN Large Hadron Collider*, *Phys. Rev. C* **92** (2015) 034906 [arXiv:1306.0121] [INSPIRE].

[32] J. Rafelski and J. Letessier, *Importance of reaction volume in hadronic collisions: canonical enhancement*, *J. Phys. G* **28** (2002) 1819 [hep-ph/0112151] [INSPIRE].

[33] K. Redlich and A. Tounsi, *Strangeness enhancement and energy dependence in heavy ion collisions*, *Eur. Phys. J. C* **24** (2002) 589 [hep-ph/0111261] [INSPIRE].

[34] S. Hamieh, K. Redlich and A. Tounsi, *Canonical description of strangeness enhancement from p-A to Pb-Pb collisions*, *Phys. Lett. B* **486** (2000) 61 [hep-ph/0006024] [INSPIRE].

[35] A. Tounsi, A. Mischke and K. Redlich, *Canonical aspects of strangeness enhancement*, *Nucl. Phys. A* **715** (2003) 565c [hep-ph/0209284] [INSPIRE].

[36] ALICE collaboration, *The ALICE experiment: a journey through QCD*, *Eur. Phys. J. C* **84** (2024) 813 [arXiv:2211.04384] [INSPIRE].

[37] ALICE collaboration, *Production of Λ and K^0_s in jets in p–Pb collisions at $\sqrt{s_{NN}} = 5.02$ TeV and pp collisions at $\sqrt{s} = 7$ TeV*, *Phys. Lett. B* **827** (2022) 136984 [arXiv:2105.04890] [INSPIRE].

[38] ALICE collaboration, *Production of K^0_S, Λ ($\bar{\Lambda}$), $\Xi^\pm$ and $\Omega^\pm$ in jets and in the underlying event in pp and p−Pb collisions*, *JHEP* **07** (2023) 136 [arXiv:2211.08936] [INSPIRE].

[39] M. Cacciari, G.P. Salam and G. Soyez, *The anti-k_t jet clustering algorithm*, *JHEP* **04** (2008) 063 [arXiv:0802.1189] [INSPIRE].

[40] M. Cacciari, G.P. Salam and G. Soyez, *FastJet user manual*, *Eur. Phys. J. C* **72** (2012) 1896 [arXiv:1111.6097] [INSPIRE].

[41] T. Sjöstrand et al., *An introduction to PYTHIA 8.2*, *Comput. Phys. Commun.* **191** (2015) 159 [arXiv:1410.3012] [INSPIRE].

[42] ALICE collaboration, *The ALICE experiment at the CERN LHC*, 2008 *JINST* **3** S08002 [INSPIRE].

JHEP09(2024)204

[43] ALICE collaboration, *Performance of the ALICE experiment at the CERN LHC*, *Int. J. Mod. Phys. A* **29** (2014) 1430044 [arXiv:1402.4476] [INSPIRE].

[44] ALICE collaboration, *ALICE technical design report of the inner tracking system (ITS)*, CERN-LHCC-99-12 (1999) [INSPIRE].

[45] ALICE collaboration, *ALICE time projection chamber: Technical Design Report*, CERN-LHCC-2000-001, CERN, Geneva (2000).

[46] ALICE collaboration, *ALICE Time-Of-Flight system (TOF): Technical Design Report*, CERN-LHCC-2000-012, CERN, Geneva (2000).

[47] ALICE collaboration, *Performance of the ALICE VZERO system*, 2013 *JINST* **8** P10016 [arXiv:1306.3130] [INSPIRE].

[48] ALICE collaboration, *Pseudorapidity distributions of charged particles as a function of mid- and forward rapidity multiplicities in pp collisions at* $\sqrt{s} = 5.02$*,* 7 *and* 13 *TeV*, *Eur. Phys. J. C* **81** (2021) 630 [arXiv:2009.09434] [INSPIRE].

[49] PARTICLE DATA GROUP collaboration, *Review of Particle Physics*, *PTEP* **2022** (2022) 083C01 [INSPIRE].

[50] ALICE collaboration, *Production of pions, kaons and protons in pp collisions at* $\sqrt{s} = 900$ *GeV with ALICE at the LHC*, *Eur. Phys. J. C* **71** (2011) 1655 [arXiv:1101.4110] [INSPIRE].

[51] GEANT4 collaboration, *GEANT4–a simulation toolkit*, *Nucl. Instrum. Meth. A* **506** (2003) 250 [INSPIRE].

[52] C. Tsallis, *Possible generalization of Boltzmann-Gibbs statistics*, *J. Statist. Phys.* **52** (1988) 479 [INSPIRE].

[53] R. Barlow, *Systematic errors: facts and fictions*, in the proceedings of the *Conference on Advanced Statistical Techniques in Particle Physics*, Durham, U.K., March 18–22 (2002) [hep-ex/0207026] [INSPIRE].

[54] B. Andersson, *The Lund Model*, Cambridge University Press (1998) [DOI:10.1017/cbo9780511524363].

[55] K. Werner, *Core-corona separation in ultra-relativistic heavy ion collisions*, *Phys. Rev. Lett.* **98** (2007) 152301 [arXiv:0704.1270] [INSPIRE].

[56] K. Werner, *Core-corona procedure and microcanonical hadronization to understand strangeness enhancement in proton-proton and heavy ion collisions in the EPOS4 framework*, *Phys. Rev. C* **109** (2024) 014910 [arXiv:2306.10277] [INSPIRE].

JHEP09(2024)204

The ALICE collaboration

S. Acharya[127], D. Adamová[86], A. Agarwal[135], G. Aglieri Rinella[32], L. Aglietta[24], M. Agnello[29], N. Agrawal[25], Z. Ahammed[135], S. Ahmad[15], S.U. Ahn[71], I. Ahuja[37], A. Akindinov[141], V. Akishina[38], M. Al-Turany[97], D. Aleksandrov[141], B. Alessandro[56], H.M. Alfanda[6], R. Alfaro Molina[67], B. Ali[15], A. Alici[25], N. Alizadehvandchali[116], A. Alkin[104], J. Alme[20], G. Alocco[52], T. Alt[64], A.R. Altamura[50], I. Altsybeev[95], J.R. Alvarado[44], C.O.R. Alvarez[44], M.N. Anaam[6], C. Andrei[45], N. Andreou[115], A. Andronic[126], E. Andronov[141], V. Anguelov[94], F. Antinori[54], P. Antonioli[51], N. Apadula[74], L. Aphecetche[103], H. Appelshäuser[64], C. Arata[73], S. Arcelli[25], M. Aresti[22], R. Arnaldi[56], J.G.M.C.A. Arneiro[110], I.C. Arsene[19], M. Arslandok[138], A. Augustinus[32], R. Averbeck[97], M.D. Azmi[15], H. Baba[124], A. Badalà[53], J. Bae[104], Y.W. Baek[40], X. Bai[120], R. Bailhache[64], Y. Bailung[48], R. Bala[91], A. Balbino[29], A. Baldisseri[130], B. Balis[2], D. Banerjee[4], Z. Banoo[91], V. Barbasova[37], F. Barile[31], L. Barioglio[56], M. Barlou[78], B. Barman[41], G.G. Barnaföldi[46], L.S. Barnby[115], E. Barreau[103], V. Barret[127], L. Barreto[110], C. Bartels[119], K. Barth[32], E. Bartsch[64], N. Bastid[127], S. Basu[75], G. Batigne[103], D. Battistini[95], B. Batyunya[142], D. Bauri[47], J.L. Bazo Alba[101], I.G. Bearden[83], C. Beattie[138], P. Becht[97], D. Behera[48], I. Belikov[129], A.D.C. Bell Hechavarria[126], F. Bellini[25], R. Bellwied[116], S. Belokurova[141], L.G.E. Beltran[109], Y.A.V. Beltran[44], G. Bencedi[46], A. Bensaoula[116], S. Beole[24], Y. Berdnikov[141], A. Berdnikova[94], L. Bergmann[94], M.G. Besoiu[63], L. Betev[32], P.P. Bhaduri[135], A. Bhasin[91], B. Bhattacharjee[41], L. Bianchi[24], N. Bianchi[49], J. Bielčík[35], J. Bielčíková[86], A.P. Bigot[129], A. Bilandzic[95], G. Biro[46], S. Biswas[4], N. Bize[103], J.T. Blair[108], D. Blau[141], M.B. Blidaru[97], N. Bluhme[38], C. Blume[64], G. Boca[21,55], F. Bock[87], T. Bodova[20], J. Bok[16], L. Boldizsár[46], M. Bombara[37], P.M. Bond[32], G. Bonomi[134,55], H. Borel[130], A. Borissov[141], A.G. Borquez Carcamo[94], H. Bossi[138], E. Botta[24], Y.E.M. Bouziani[64], L. Bratrud[64], P. Braun-Munzinger[97], M. Bregant[110], M. Broz[35], G.E. Bruno[96,31], V.D. Buchakchiev[36], M.D. Buckland[23], D. Budnikov[141], H. Buesching[64], S. Bufalino[29], P. Buhler[102], N. Burmasov[141], Z. Buthelezi[68,123], A. Bylinkin[20], S.A. Bysiak[107], J.C. Cabanillas Noris[109], M.F.T. Cabrera[116], M. Cai[6], H. Caines[138], A. Caliva[28], E. Calvo Villar[101], J.M.M. Camacho[109], P. Camerini[23], F.D.M. Canedo[110], S.L. Cantway[138], M. Carabas[113], A.A. Carballo[32], F. Carnesecchi[32], R. Caron[128], L.A.D. Carvalho[110], J. Castillo Castellanos[130], M. Castoldi[32], F. Catalano[32], S. Cattaruzzi[23], C. Ceballos Sanchez[142], R. Cerri[24], I. Chakaberia[74], P. Chakraborty[136,47], S. Chandra[135], S. Chapeland[32], M. Chartier[119], S. Chattopadhay[135], S. Chattopadhyay[135], S. Chattopadhyay[99], M. Chen[39], T. Cheng[97,6], C. Cheshkov[128], V. Chibante Barroso[32], D.D. Chinellato[111], E.S. Chizzali[II,95], J. Cho[58], S. Cho[58], P. Chochula[32], Z.A. Chochulska[136], D. Choudhury[41], P. Christakoglou[84], C.H. Christensen[83], P. Christiansen[75], T. Chujo[125], M. Ciacco[29], C. Cicalo[52], M.R. Ciupek[97], G. Clai[III,51], F. Colamaria[50], J.S. Colburn[100], D. Colella[31], M. Colocci[25], M. Concas[32], G. Conesa Balbastre[73], Z. Conesa del Valle[131], G. Contin[23], J.G. Contreras[35], M.L. Coquet[103,130], P. Cortese[133,56], M.R. Cosentino[112], F. Costa[32], S. Costanza[21,55], C. Cot[131], J. Crkovská[94], P. Crochet[127], R. Cruz-Torres[74], P. Cui[6], M.M. Czarnynoga[136], A. Dainese[54], G. Dange[38], M.C. Danisch[94], A. Danu[63], P. Das[80], P. Das[4], S. Das[4],

JHEP09(2024)204

A.R. Dash[126], S. Dash[47], A. De Caro[28], G. de Cataldo[50], J. de Cuveland[38], A. De Falco[22], D. De Gruttola[28], N. De Marco[56], C. De Martin[23], S. De Pasquale[28], R. Deb[134], R. Del Grande[95], L. Dello Stritto[32], W. Deng[6], K.C. Devereaux[18], P. Dhankher[18], D. Di Bari[31], A. Di Mauro[32], B. Diab[130], R.A. Diaz[142,7], T. Dietel[114], Y. Ding[6], J. Ditzel[64], R. Divià[32], Ø. Djuvsland[20], U. Dmitrieva[141], A. Dobrin[63], B. Dönigus[64], J.M. Dubinski[136], A. Dubla[97], P. Dupieux[127], N. Dzalaiova[13], T.M. Eder[126], R.J. Ehlers[74], F. Eisenhut[64], R. Ejima[92], D. Elia[50], B. Erazmus[103], F. Ercolessi[25], B. Espagnon[131], G. Eulisse[32], D. Evans[100], S. Evdokimov[141], L. Fabbietti[95], M. Faggin[23], J. Faivre[73], F. Fan[6], W. Fan[74], A. Fantoni[49], M. Fasel[87], A. Feliciello[56], G. Feofilov[141], A. Fernández Téllez[44], L. Ferrandi[110], M.B. Ferrer[32], A. Ferrero[130], C. Ferrero[IV,56], A. Ferretti[24], V.J.G. Feuillard[94], V. Filova[35], D. Finogeev[141], F.M. Fionda[52], E. Flatland[32], F. Flor[138,116], A.N. Flores[108], S. Foertsch[68], I. Fokin[94], S. Fokin[141], U. Follo[IV,56], E. Fragiacomo[57], E. Frajna[46], U. Fuchs[32], N. Funicello[28], C. Furget[73], A. Furs[141], T. Fusayasu[98], J.J. Gaardhøje[83], M. Gagliardi[24], A.M. Gago[101], T. Gahlaut[47], C.D. Galvan[109], D.R. Gangadharan[116], P. Ganoti[78], C. Garabatos[97], J.M. Garcia[44], T. García Chávez[44], E. Garcia-Solis[9], C. Gargiulo[32], P. Gasik[97], H.M. Gaur[38], A. Gautam[118], M.B. Gay Ducati[66], M. Germain[103], C. Ghosh[135], M. Giacalone[51], G. Gioachin[29], P. Giubellino[97,56], P. Giubilato[27], A.M.C. Glaenzer[130], P. Glässel[94], E. Glimos[122], D.J.Q. Goh[76], V. Gonzalez[137], P. Gordeev[141], M. Gorgon[2], K. Goswami[48], S. Gotovac[33], V. Grabski[67], L.K. Graczykowski[136], E. Grecka[86], A. Grelli[59], C. Grigoras[32], V. Grigoriev[141], S. Grigoryan[142,1], F. Grosa[32], J.F. Grosse-Oetringhaus[32], R. Grosso[97], D. Grund[35], N.A. Grunwald[94], G.G. Guardiano[111], R. Guernane[73], M. Guilbaud[103], K. Gulbrandsen[83], J.J.W.K. Gumprecht[102], T. Gündem[64], T. Gunji[124], W. Guo[6], A. Gupta[91], R. Gupta[91], R. Gupta[48], K. Gwizdziel[136], L. Gyulai[46], C. Hadjidakis[131], F.U. Haider[91], S. Haidlova[35], M. Haldar[4], H. Hamagaki[76], A. Hamdi[74], Y. Han[139], B.G. Hanley[137], R. Hannigan[108], J. Hansen[75], M.R. Haque[97], J.W. Harris[138], A. Harton[9], M.V. Hartung[64], H. Hassan[117], D. Hatzifotiadou[51], P. Hauer[42], L.B. Havener[138], E. Hellbär[97], H. Helstrup[34], M. Hemmer[64], T. Herman[35], S.G. Hernandez[116], G. Herrera Corral[8], S. Herrmann[128], K.F. Hetland[34], B. Heybeck[64], H. Hillemanns[32], B. Hippolyte[129], F.W. Hoffmann[70], B. Hofman[59], G.H. Hong[139], M. Horst[95], A. Horzyk[2], Y. Hou[6], P. Hristov[32], P. Huhn[64], L.M. Huhta[117], T.J. Humanic[88], A. Hutson[116], D. Hutter[38], M.C. Hwang[18], R. Ilkaev[141], M. Inaba[125], G.M. Innocenti[32], M. Ippolitov[141], A. Isakov[84], T. Isidori[118], M.S. Islam[99], S. Iurchenko[141], M. Ivanov[13], M. Ivanov[97], V. Ivanov[141], K.E. Iversen[75], M. Jablonski[2], B. Jacak[18,74], N. Jacazio[25], P.M. Jacobs[74], S. Jadlovska[106], J. Jadlovsky[106], S. Jaelani[82], C. Jahnke[110], M.J. Jakubowska[136], M.A. Janik[136], T. Janson[70], S. Ji[16], S. Jia[10], A.A.P. Jimenez[65], F. Jonas[74], D.M. Jones[119], J.M. Jowett[32,97], J. Jung[64], M. Jung[64], A. Junique[32], A. Jusko[100], J. Kaewjai[105], P. Kalinak[60], A. Kalweit[32], A. Karasu Uysal[V,72], D. Karatovic[89], N. Karatzenis[100], O. Karavichev[141], T. Karavicheva[141], E. Karpechev[141], M.J. Karwowska[32,136], U. Kebschull[70], R. Keidel[140], M. Keil[32], B. Ketzer[42], S.S. Khade[48], A.M. Khan[120], S. Khan[15], A. Khanzadeev[141], Y. Kharlov[141], A. Khatun[118], A. Khuntia[35], Z. Khuranova[64], B. Kileng[34], B. Kim[104], C. Kim[16], D.J. Kim[117], E.J. Kim[69], J. Kim[139], J. Kim[58], J. Kim[32,69], M. Kim[18], S. Kim[17],

JHEP09(2024)204

T. Kim[139], K. Kimura[92], A. Kirkova[36], S. Kirsch[64], I. Kisel[38], S. Kiselev[141], A. Kisiel[136], J.P. Kitowski[2], J.L. Klay[5], J. Klein[32], S. Klein[74], C. Klein-Bösing[126], M. Kleiner[64], T. Klemenz[95], A. Kluge[32], C. Kobdaj[105], R. Kohara[124], T. Kollegger[97], A. Kondratyev[142], N. Kondratyeva[141], J. Konig[64], S.A. Konigstorfer[95], P.J. Konopka[32], G. Kornakov[136], M. Korwieser[95], S.D. Koryciak[2], C. Koster[84], A. Kotliarov[86], N. Kovacic[89], V. Kovalenko[141], M. Kowalski[107], V. Kozhuharov[36], I. Králik[60], A. Kravčáková[37], L. Krcal[32,38], M. Krivda[100,60], F. Krizek[86], K. Krizkova Gajdosova[32], C. Krug[66], M. Krüger[64], D.M. Krupova[35], E. Kryshen[141], V. Kučera[58], C. Kuhn[129], P.G. Kuijer[84], T. Kumaoka[125], D. Kumar[135], L. Kumar[90], N. Kumar[90], S. Kumar[31], S. Kundu[32], P. Kurashvili[79], A. Kurepin[141], A.B. Kurepin[141], A. Kuryakin[141], S. Kushpil[86], V. Kuskov[141], M. Kutyla[136], A. Kuznetsov[142], M.J. Kweon[58], Y. Kwon[139], S.L. La Pointe[38], P. La Rocca[26], A. Lakrathok[105], M. Lamanna[32], A.R. Landou[73], R. Langoy[121], P. Larionov[32], E. Laudi[32], L. Lautner[32,95], R.A.N. Laveaga[109], R. Lavicka[102], R. Lea[134,55], H. Lee[104], I. Legrand[45], G. Legras[126], J. Lehrbach[38], A.M. Lejeune[35], T.M. Lelek[2], R.C. Lemmon[I,85], I. León Monzón[109], M.M. Lesch[95], E.D. Lesser[18], P. Lévai[46], M. Li[6], X. Li[10], B.E. Liang-gilman[18], J. Lien[121], R. Lietava[100], I. Likmeta[116], B. Lim[24], S.H. Lim[16], V. Lindenstruth[38], A. Lindner[45], C. Lippmann[97], D.H. Liu[6], J. Liu[119], G.S.S. Liveraro[111], I.M. Lofnes[20], C. Loizides[87], S. Lokos[107], J. Lömker[59], X. Lopez[127], E. López Torres[7], P. Lu[97,120], F.V. Lugo[67], J.R. Luhder[126], M. Lunardon[27], G. Luparello[57], Y.G. Ma[39], M. Mager[32], A. Maire[129], E.M. Majerz[2], M.V. Makariev[36], M. Malaev[141], G. Malfattore[25], N.M. Malik[91], Q.W. Malik[19], S.K. Malik[91], L. Malinina[I,VIII,142], D. Mallick[131], N. Mallick[48], G. Mandaglio[30,53], S.K. Mandal[79], A. Manea[63], V. Manko[141], F. Manso[127], V. Manzari[50], Y. Mao[6], R.W. Marcjan[2], G.V. Margagliotti[23], A. Margotti[51], A. Marín[97], C. Markert[108], P. Martinengo[32], M.I. Martínez[44], G. Martínez García[103], M.P.P. Martins[110], S. Masciocchi[97], M. Masera[24], A. Masoni[52], L. Massacrier[131], O. Massen[59], A. Mastroserio[132,50], O. Matonoha[75], S. Mattiazzo[27], A. Matyja[107], A.L. Mazuecos[32], F. Mazzaschi[32,24], M. Mazzilli[116], J.E. Mdhluli[123], Y. Melikyan[43], M. Melo[110], A. Menchaca-Rocha[67], J.E.M. Mendez[65], E. Meninno[102], A.S. Menon[116], M.W. Menzel[32,94], M. Meres[13], Y. Miake[125], L. Micheletti[32], D.L. Mihaylov[95], K. Mikhaylov[142,141], N. Minafra[118], D. Miśkowiec[97], A. Modak[134,4], B. Mohanty[80], M. Mohisin Khan[VI,15], M.A. Molander[43], S. Monira[136], C. Mordasini[117], D.A. Moreira De Godoy[126], I. Morozov[141], A. Morsch[32], T. Mrnjavac[32], V. Muccifora[49], S. Muhuri[135], J.D. Mulligan[74], A. Mulliri[22], M.G. Munhoz[110], R.H. Munzer[64], H. Murakami[124], S. Murray[114], L. Musa[32], J. Musinsky[60], J.W. Myrcha[136], B. Naik[123], A.I. Nambrath[18], B.K. Nandi[47], R. Nania[51], E. Nappi[50], A.F. Nassirpour[17], A. Nath[94], C. Nattrass[122], M.N. Naydenov[36], A. Neagu[19], A. Negru[113], E. Nekrasova[141], L. Nellen[65], R. Nepeivoda[75], S. Nese[19], G. Neskovic[38], N. Nicassio[50], B.S. Nielsen[83], E.G. Nielsen[83], S. Nikolaev[141], S. Nikulin[141], V. Nikulin[141], F. Noferini[51], S. Noh[12], P. Nomokonov[142], J. Norman[119], N. Novitzky[87], P. Nowakowski[136], A. Nyanin[141], J. Nystrand[20], S. Oh[17], A. Ohlson[75], V.A. Okorokov[141], J. Oleniacz[136], A. Onnerstad[117], C. Oppedisano[56], A. Ortiz Velasquez[65], J. Otwinowski[107], M. Oya[92], K. Oyama[76], Y. Pachmayer[94], S. Padhan[47], D. Pagano[134,55], G. Paić[65], S. Paisano-Guzmán[44], A. Palasciano[50], S. Panebianco[130], C. Pantouvakis[27], H. Park[125], H. Park[104], J. Park[125], J.E. Parkkila[32], Y. Patley[47], B. Paul[22], H. Pei[6],

JHEP09(2024)204

T. Peitzmann[59], X. Peng[11], M. Pennisi[24], S. Perciballi[24], D. Peresunko[141], G.M. Perez[7], Y. Pestov[141], M.T. Petersen[83], V. Petrov[141], M. Petrovici[45], S. Piano[57], M. Pikna[13], P. Pillot[103], O. Pinazza[51,32], L. Pinsky[116], C. Pinto[95], S. Pisano[49], M. Płoskoń[74], M. Planinic[89], F. Pliquett[64], M.G. Poghosyan[87], B. Polichtchouk[141], S. Politano[29], N. Poljak[89], A. Pop[45], S. Porteboeuf-Houssais[127], V. Pozdniakov[I,142], I.Y. Pozos[44], K.K. Pradhan[48], S.K. Prasad[4], S. Prasad[48], R. Preghenella[51], F. Prino[56], C.A. Pruneau[137], I. Pshenichnov[141], M. Puccio[32], S. Pucillo[24], S. Qiu[84], L. Quaglia[24], S. Ragoni[14], A. Rai[138], A. Rakotozafindrabe[130], L. Ramello[133,56], F. Rami[129], M. Rasa[26], S.S. Räsänen[43], R. Rath[51], M.P. Rauch[20], I. Ravasenga[32], K.F. Read[87,122], C. Reckziegel[112], A.R. Redelbach[38], K. Redlich[VII,79], C.A. Reetz[97], H.D. Regules-Medel[44], A. Rehman[20], F. Reidt[32], H.A. Reme-Ness[34], Z. Rescakova[37], K. Reygers[94], A. Riabov[141], V. Riabov[141], R. Ricci[28], M. Richter[20], A.A. Riedel[95], W. Riegler[32], A.G. Riffero[24], C. Ripoli[28], C. Ristea[63], M.V. Rodriguez[32], M. Rodríguez Cahuantzi[44], S.A. Rodríguez Ramírez[44], K. Røed[19], R. Rogalev[141], E. Rogochaya[142], T.S. Rogoschinski[64], D. Rohr[32], D. Röhrich[20], S. Rojas Torres[35], P.S. Rokita[136], G. Romanenko[25], F. Ronchetti[49], E.D. Rosas[65], K. Roslon[136], A. Rossi[54], A. Roy[48], S. Roy[47], N. Rubini[25], J.A. Rudolph[84], D. Ruggiano[136], R. Rui[23], P.G. Russek[2], R. Russo[84], A. Rustamov[81], E. Ryabinkin[141], Y. Ryabov[141], A. Rybicki[107], J. Ryu[16], W. Rzesa[136], S. Sadhu[31], S. Sadovsky[141], J. Saetre[20], K. Šafařík[35], S.K. Saha[4], S. Saha[80], B. Sahoo[48], R. Sahoo[48], S. Sahoo[61], D. Sahu[48], P.K. Sahu[61], J. Saini[135], K. Sajdakova[37], S. Sakai[125], M.P. Salvan[97], S. Sambyal[91], D. Samitz[102], I. Sanna[32,95], T.B. Saramela[110], D. Sarkar[83], P. Sarma[41], V. Sarritzu[22], V.M. Sarti[95], M.H.P. Sas[32], S. Sawan[80], E. Scapparone[51], J. Schambach[87], H.S. Scheid[64], C. Schiaua[45], R. Schicker[94], F. Schlepper[94], A. Schmah[97], C. Schmidt[97], H.R. Schmidt[93], M.O. Schmidt[32], M. Schmidt[93], N.V. Schmidt[87], A.R. Schmier[122], R. Schotter[129], A. Schröter[38], J. Schukraft[32], K. Schweda[97], G. Scioli[25], E. Scomparin[56], J.E. Seger[14], Y. Sekiguchi[124], D. Sekihata[124], M. Selina[84], I. Selyuzhenkov[97], S. Senyukov[129], J.J. Seo[94], D. Serebryakov[141], L. Serkin[65], L. Šerkšnytė[95], A. Sevcenco[63], T.J. Shaba[68], A. Shabetai[103], R. Shahoyan[32], A. Shangaraev[141], B. Sharma[91], D. Sharma[47], H. Sharma[54], M. Sharma[91], S. Sharma[76], S. Sharma[91], U. Sharma[91], A. Shatat[131], O. Sheibani[116], K. Shigaki[92], M. Shimomura[77], J. Shin[12], S. Shirinkin[141], Q. Shou[39], Y. Sibiriak[141], S. Siddhanta[52], T. Siemiarczuk[79], T.F. Silva[110], D. Silvermyr[75], T. Simantathammakul[105], R. Simeonov[36], B. Singh[91], B. Singh[95], K. Singh[48], R. Singh[80], R. Singh[91], R. Singh[97,48], S. Singh[15], V.K. Singh[135], V. Singhal[135], T. Sinha[99], B. Sitar[13], M. Sitta[133,56], T.B. Skaali[19], G. Skorodumovs[94], N. Smirnov[138], R.J.M. Snellings[59], E.H. Solheim[19], J. Song[16], C. Sonnabend[32,97], J.M. Sonneveld[84], F. Soramel[27], A.B. Soto-hernandez[88], R. Spijkers[84], I. Sputowska[107], J. Staa[75], J. Stachel[94], I. Stan[63], P.J. Steffanic[122], S.F. Stiefelmaier[94], D. Stocco[103], I. Storehaug[19], N.J. Strangmann[64], P. Stratmann[126], S. Strazzi[25], A. Sturniolo[30,53], C.P. Stylianidis[84], A.A.P. Suaide[110], C. Suire[131], M. Sukhanov[141], M. Suljic[32], R. Sultanov[141], V. Sumberia[91], S. Sumowidagdo[82], I. Szarka[13], M. Szymkowski[136], S.F. Taghavi[95], G. Taillepied[97], J. Takahashi[111], G.J. Tambave[80], S. Tang[6], Z. Tang[120], J.D. Tapia Takaki[118], N. Tapus[113], L.A. Tarasovicova[126], M.G. Tarzila[45], G.F. Tassielli[31], A. Tauro[32], A. Tavira García[131], G. Tejeda Muñoz[44],

JHEP09(2024)204

A. Telesca[32], L. Terlizzi[24], C. Terrevoli[50], S. Thakur[4], D. Thomas[108], A. Tikhonov[141], N. Tiltmann[32,126], A.R. Timmins[116], M. Tkacik[106], T. Tkacik[106], A. Toia[64], R. Tokumoto[92], S. Tomassini[25], K. Tomohiro[92], N. Topilskaya[141], M. Toppi[49], T. Tork[131], V.V. Torres[103], A.G. Torres Ramos[31], A. Trifiró[30,53], T. Triloki[96], A.S. Triolo[32,30,53], S. Tripathy[32], T. Tripathy[47], V. Trubnikov[3], W.H. Trzaska[117], T.P. Trzcinski[136], C. Tsolanta[19], R. Tu[39], A. Tumkin[141], R. Turrisi[54], T.S. Tveter[19], K. Ullaland[20], B. Ulukutlu[95], A. Uras[128], M. Urioni[134], G.L. Usai[22], M. Vala[37], N. Valle[55], L.V.R. van Doremalen[59], M. van Leeuwen[84], C.A. van Veen[94], R.J.G. van Weelden[84], P. Vande Vyvre[32], D. Varga[46], Z. Varga[46], P. Vargas Torres[65], M. Vasileiou[78], A. Vasiliev[141], O. Vázquez Doce[49], O. Vazquez Rueda[116], V. Vechernin[141], E. Vercellin[24], S. Vergara Limón[44], R. Verma[47], L. Vermunt[97], R. Vértesi[46], M. Verweij[59], L. Vickovic[33], Z. Vilakazi[123], O. Villalobos Baillie[100], A. Villani[23], A. Vinogradov[141], T. Virgili[28], M.M.O. Virta[117], V. Vislavicius[75], A. Vodopyanov[142], B. Volkel[32], M.A. Völkl[94], S.A. Voloshin[137], G. Volpe[31], B. von Haller[32], I. Vorobyev[32], N. Vozniuk[141], J. Vrláková[37], J. Wan[39], C. Wang[39], D. Wang[39], Y. Wang[39], Y. Wang[6], A. Wegrzynek[32], F.T. Weiglhofer[38], S.C. Wenzel[32], J.P. Wessels[126], J. Wiechula[64], J. Wikne[19], G. Wilk[79], J. Wilkinson[97], G.A. Willems[126], B. Windelband[94], M. Winn[130], J.R. Wright[108], W. Wu[39], Y. Wu[120], Z. Xiong[120], R. Xu[6], A. Yadav[42], A.K. Yadav[135], Y. Yamaguchi[92], S. Yang[20], S. Yano[92], E.R. Yeats[18], Z. Yin[6], I.-K. Yoo[16], J.H. Yoon[58], H. Yu[12], S. Yuan[20], A. Yuncu[94], V. Zaccolo[23], C. Zampolli[32], F. Zanone[94], N. Zardoshti[32], A. Zarochentsev[141], P. Závada[62], N. Zaviyalov[141], M. Zhalov[141], B. Zhang[6], C. Zhang[130], L. Zhang[39], M. Zhang[127,6], M. Zhang[6], S. Zhang[39], X. Zhang[6], Y. Zhang[120], Z. Zhang[6], M. Zhao[10], V. Zherebchevskii[141], Y. Zhi[10], D. Zhou[6], Y. Zhou[83], J. Zhu[54,6], S. Zhu[120], Y. Zhu[6], S.C. Zugravel[56], N. Zurlo[134,55]

[1] *A.I. Alikhanyan National Science Laboratory (Yerevan Physics Institute) Foundation, Yerevan, Armenia*
[2] *AGH University of Krakow, Cracow, Poland*
[3] *Bogolyubov Institute for Theoretical Physics, National Academy of Sciences of Ukraine, Kiev, Ukraine*
[4] *Bose Institute, Department of Physics and Centre for Astroparticle Physics and Space Science (CAPSS), Kolkata, India*
[5] *California Polytechnic State University, San Luis Obispo, California, United States*
[6] *Central China Normal University, Wuhan, China*
[7] *Centro de Aplicaciones Tecnológicas y Desarrollo Nuclear (CEADEN), Havana, Cuba*
[8] *Centro de Investigación y de Estudios Avanzados (CINVESTAV), Mexico City and Mérida, Mexico*
[9] *Chicago State University, Chicago, Illinois, United States*
[10] *China Institute of Atomic Energy, Beijing, China*
[11] *China University of Geosciences, Wuhan, China*
[12] *Chungbuk National University, Cheongju, Republic of Korea*
[13] *Comenius University Bratislava, Faculty of Mathematics, Physics and Informatics, Bratislava, Slovak Republic*
[14] *Creighton University, Omaha, Nebraska, United States*
[15] *Department of Physics, Aligarh Muslim University, Aligarh, India*
[16] *Department of Physics, Pusan National University, Pusan, Republic of Korea*
[17] *Department of Physics, Sejong University, Seoul, Republic of Korea*
[18] *Department of Physics, University of California, Berkeley, California, United States*
[19] *Department of Physics, University of Oslo, Oslo, Norway*
[20] *Department of Physics and Technology, University of Bergen, Bergen, Norway*
[21] *Dipartimento di Fisica, Università di Pavia, Pavia, Italy*
[22] *Dipartimento di Fisica dell'Università and Sezione INFN, Cagliari, Italy*

JHEP09(2024)204

[23] Dipartimento di Fisica dell'Università and Sezione INFN, Trieste, Italy
[24] Dipartimento di Fisica dell'Università and Sezione INFN, Turin, Italy
[25] Dipartimento di Fisica e Astronomia dell'Università and Sezione INFN, Bologna, Italy
[26] Dipartimento di Fisica e Astronomia dell'Università and Sezione INFN, Catania, Italy
[27] Dipartimento di Fisica e Astronomia dell'Università and Sezione INFN, Padova, Italy
[28] Dipartimento di Fisica 'E.R. Caianiello' dell'Università and Gruppo Collegato INFN, Salerno, Italy
[29] Dipartimento DISAT del Politecnico and Sezione INFN, Turin, Italy
[30] Dipartimento di Scienze MIFT, Università di Messina, Messina, Italy
[31] Dipartimento Interateneo di Fisica 'M. Merlin' and Sezione INFN, Bari, Italy
[32] European Organization for Nuclear Research (CERN), Geneva, Switzerland
[33] Faculty of Electrical Engineering, Mechanical Engineering and Naval Architecture, University of Split, Split, Croatia
[34] Faculty of Engineering and Science, Western Norway University of Applied Sciences, Bergen, Norway
[35] Faculty of Nuclear Sciences and Physical Engineering, Czech Technical University in Prague, Prague, Czech Republic
[36] Faculty of Physics, Sofia University, Sofia, Bulgaria
[37] Faculty of Science, P.J. Šafárik University, Košice, Slovak Republic
[38] Frankfurt Institute for Advanced Studies, Johann Wolfgang Goethe-Universität Frankfurt, Frankfurt, Germany
[39] Fudan University, Shanghai, China
[40] Gangneung-Wonju National University, Gangneung, Republic of Korea
[41] Gauhati University, Department of Physics, Guwahati, India
[42] Helmholtz-Institut für Strahlen- und Kernphysik, Rheinische Friedrich-Wilhelms-Universität Bonn, Bonn, Germany
[43] Helsinki Institute of Physics (HIP), Helsinki, Finland
[44] High Energy Physics Group, Universidad Autónoma de Puebla, Puebla, Mexico
[45] Horia Hulubei National Institute of Physics and Nuclear Engineering, Bucharest, Romania
[46] HUN-REN Wigner Research Centre for Physics, Budapest, Hungary
[47] Indian Institute of Technology Bombay (IIT), Mumbai, India
[48] Indian Institute of Technology Indore, Indore, India
[49] INFN, Laboratori Nazionali di Frascati, Frascati, Italy
[50] INFN, Sezione di Bari, Bari, Italy
[51] INFN, Sezione di Bologna, Bologna, Italy
[52] INFN, Sezione di Cagliari, Cagliari, Italy
[53] INFN, Sezione di Catania, Catania, Italy
[54] INFN, Sezione di Padova, Padova, Italy
[55] INFN, Sezione di Pavia, Pavia, Italy
[56] INFN, Sezione di Torino, Turin, Italy
[57] INFN, Sezione di Trieste, Trieste, Italy
[58] Inha University, Incheon, Republic of Korea
[59] Institute for Gravitational and Subatomic Physics (GRASP), Utrecht University/Nikhef, Utrecht, Netherlands
[60] Institute of Experimental Physics, Slovak Academy of Sciences, Košice, Slovak Republic
[61] Institute of Physics, Homi Bhabha National Institute, Bhubaneswar, India
[62] Institute of Physics of the Czech Academy of Sciences, Prague, Czech Republic
[63] Institute of Space Science (ISS), Bucharest, Romania
[64] Institut für Kernphysik, Johann Wolfgang Goethe-Universität Frankfurt, Frankfurt, Germany
[65] Instituto de Ciencias Nucleares, Universidad Nacional Autónoma de México, Mexico City, Mexico
[66] Instituto de Física, Universidade Federal do Rio Grande do Sul (UFRGS), Porto Alegre, Brazil
[67] Instituto de Física, Universidad Nacional Autónoma de México, Mexico City, Mexico
[68] iThemba LABS, National Research Foundation, Somerset West, South Africa
[69] Jeonbuk National University, Jeonju, Republic of Korea
[70] Johann-Wolfgang-Goethe Universität Frankfurt Institut für Informatik, Fachbereich Informatik und

JHEP09(2024)204

Mathematik, Frankfurt, Germany
[71] *Korea Institute of Science and Technology Information, Daejeon, Republic of Korea*
[72] *KTO Karatay University, Konya, Turkey*
[73] *Laboratoire de Physique Subatomique et de Cosmologie, Université Grenoble-Alpes, CNRS-IN2P3, Grenoble, France*
[74] *Lawrence Berkeley National Laboratory, Berkeley, California, United States*
[75] *Lund University Department of Physics, Division of Particle Physics, Lund, Sweden*
[76] *Nagasaki Institute of Applied Science, Nagasaki, Japan*
[77] *Nara Women's University (NWU), Nara, Japan*
[78] *National and Kapodistrian University of Athens, School of Science, Department of Physics , Athens, Greece*
[79] *National Centre for Nuclear Research, Warsaw, Poland*
[80] *National Institute of Science Education and Research, Homi Bhabha National Institute, Jatni, India*
[81] *National Nuclear Research Center, Baku, Azerbaijan*
[82] *National Research and Innovation Agency - BRIN, Jakarta, Indonesia*
[83] *Niels Bohr Institute, University of Copenhagen, Copenhagen, Denmark*
[84] *Nikhef, National institute for subatomic physics, Amsterdam, Netherlands*
[85] *Nuclear Physics Group, STFC Daresbury Laboratory, Daresbury, United Kingdom*
[86] *Nuclear Physics Institute of the Czech Academy of Sciences, Husinec-Řež, Czech Republic*
[87] *Oak Ridge National Laboratory, Oak Ridge, Tennessee, United States*
[88] *Ohio State University, Columbus, Ohio, United States*
[89] *Physics department, Faculty of science, University of Zagreb, Zagreb, Croatia*
[90] *Physics Department, Panjab University, Chandigarh, India*
[91] *Physics Department, University of Jammu, Jammu, India*
[92] *Physics Program and International Institute for Sustainability with Knotted Chiral Meta Matter (SKCM2), Hiroshima University, Hiroshima, Japan*
[93] *Physikalisches Institut, Eberhard-Karls-Universität Tübingen, Tübingen, Germany*
[94] *Physikalisches Institut, Ruprecht-Karls-Universität Heidelberg, Heidelberg, Germany*
[95] *Physik Department, Technische Universität München, Munich, Germany*
[96] *Politecnico di Bari and Sezione INFN, Bari, Italy*
[97] *Research Division and ExtreMe Matter Institute EMMI, GSI Helmholtzzentrum für Schwerionenforschung GmbH, Darmstadt, Germany*
[98] *Saga University, Saga, Japan*
[99] *Saha Institute of Nuclear Physics, Homi Bhabha National Institute, Kolkata, India*
[100] *School of Physics and Astronomy, University of Birmingham, Birmingham, United Kingdom*
[101] *Sección Física, Departamento de Ciencias, Pontificia Universidad Católica del Perú, Lima, Peru*
[102] *Stefan Meyer Institut für Subatomare Physik (SMI), Vienna, Austria*
[103] *SUBATECH, IMT Atlantique, Nantes Université, CNRS-IN2P3, Nantes, France*
[104] *Sungkyunkwan University, Suwon City, Republic of Korea*
[105] *Suranaree University of Technology, Nakhon Ratchasima, Thailand*
[106] *Technical University of Košice, Košice, Slovak Republic*
[107] *The Henryk Niewodniczanski Institute of Nuclear Physics, Polish Academy of Sciences, Cracow, Poland*
[108] *The University of Texas at Austin, Austin, Texas, United States*
[109] *Universidad Autónoma de Sinaloa, Culiacán, Mexico*
[110] *Universidade de São Paulo (USP), São Paulo, Brazil*
[111] *Universidade Estadual de Campinas (UNICAMP), Campinas, Brazil*
[112] *Universidade Federal do ABC, Santo Andre, Brazil*
[113] *Universitatea Nationala de Stiinta si Tehnologie Politehnica Bucuresti, Bucharest, Romania*
[114] *University of Cape Town, Cape Town, South Africa*
[115] *University of Derby, Derby, United Kingdom*
[116] *University of Houston, Houston, Texas, United States*
[117] *University of Jyväskylä, Jyväskylä, Finland*
[118] *University of Kansas, Lawrence, Kansas, United States*

JHEP09(2024)204

[119] University of Liverpool, Liverpool, United Kingdom
[120] University of Science and Technology of China, Hefei, China
[121] University of South-Eastern Norway, Kongsberg, Norway
[122] University of Tennessee, Knoxville, Tennessee, United States
[123] University of the Witwatersrand, Johannesburg, South Africa
[124] University of Tokyo, Tokyo, Japan
[125] University of Tsukuba, Tsukuba, Japan
[126] Universität Münster, Institut für Kernphysik, Münster, Germany
[127] Université Clermont Auvergne, CNRS/IN2P3, LPC, Clermont-Ferrand, France
[128] Université de Lyon, CNRS/IN2P3, Institut de Physique des 2 Infinis de Lyon, Lyon, France
[129] Université de Strasbourg, CNRS, IPHC UMR 7178, F-67000 Strasbourg, France, Strasbourg, France
[130] Université Paris-Saclay, Centre d'Etudes de Saclay (CEA), IRFU, Département de Physique Nucléaire (DPhN), Saclay, France
[131] Université Paris-Saclay, CNRS/IN2P3, IJCLab, Orsay, France
[132] Università degli Studi di Foggia, Foggia, Italy
[133] Università del Piemonte Orientale, Vercelli, Italy
[134] Università di Brescia, Brescia, Italy
[135] Variable Energy Cyclotron Centre, Homi Bhabha National Institute, Kolkata, India
[136] Warsaw University of Technology, Warsaw, Poland
[137] Wayne State University, Detroit, Michigan, United States
[138] Yale University, New Haven, Connecticut, United States
[139] Yonsei University, Seoul, Republic of Korea
[140] Zentrum für Technologie und Transfer (ZTT), Worms, Germany
[141] Affiliated with an institute covered by a cooperation agreement with CERN
[142] Affiliated with an international laboratory covered by a cooperation agreement with CERN.

[I] Deceased
[II] Also at: Max-Planck-Institut fur Physik, Munich, Germany
[III] Also at: Italian National Agency for New Technologies, Energy and Sustainable Economic Development (ENEA), Bologna, Italy
[IV] Also at: Dipartimento DET del Politecnico di Torino, Turin, Italy
[V] Also at: Yildiz Technical University, Istanbul, Türkiye
[VI] Also at: Department of Applied Physics, Aligarh Muslim University, Aligarh, India
[VII] Also at: Institute of Theoretical Physics, University of Wroclaw, Poland
[VIII] Also at: An institution covered by a cooperation agreement with CERN

JHEP09(2024)204